TRIBHUVAN UNIVERSITY

INSTITUTE OF ENGINEERING

PULCHOWK CAMPUS

B-075-BME–2075/2079

DESIGN AND ANALYSIS OF CHASSIS FRAME FOR ELECTRIC VEHICLE USING FINITE ELEMENT ANALYSIS

Submitted By:

Aarati Kunwar (075BME002)

Dikshit Guragai (075BME017)

Manisha Aryal (075BME026)

A PROJECT REPORT

SUBMITTED TO THE DEPARTMENT OF MECHANICAL AND AEROSPACE ENGINEERING IN PARTIAL FULFILLMENT OF THE REQUIREMENTS FOR THE DEGREE OF BACHELOR IN MECHANICAL ENGINEERING

DEPARTMENT OF MECHANICAL AND AEROSPACE ENGINEERING

LALITPUR, NEPAL

April, 2023

COPYRIGHT

TRIBHUVAN UNIVERSITY

INSTITUTE OF ENGINEERING

PULCHOWK CAMPUS

DEPARTMENT OF MECHANICAL AND AEROSPACE ENGINEERING

The undersigned certify that they have read, and recommended to the Institute of Engineering for acceptance, a project report entitled **"DESIGN AND ANALYSIS OF CHASSIS FRAME FOR ELECTRIC VEHICLE USING FINITE ELEMENT ANALYSIS"** submitted by Aarati Kunwar, Dikshit Guragai, and Manisha Aryal in partial fulfilment of the requirements for the degree of Bachelor of Mechanical Engineering.

_____

Supervisor, Assoc. Prof. Rajesh Kaji Kayastha
Department of Mechanical and Aerospace Engineering
Pulchowk Campus

_____

Supervisor,Assoc. Prof.Dr.Nawraj Bhattrai
Department of Mechanical and Aerospace Engineering
Pulchowk Campus

_____

External Examiner, Er.Pradhumna Adhikari
Deputy Manager
CAAN

_____

Head of Department
Department of Mechanical and Aerospace Engineering
Pulchowk Campus

Date _____

ACKNOWLEDGEMENT

First and foremost, we would like to convey our deep gratitude to all of our teachers for their consistent guidance and invaluable support. It would have been a challenging road for us without their great supervision and advice. We would like to extend our deep gratitude towards our supervisors **Dr. Nawaraj Bhattrai,** and **Assoc. Prof. Rajesh Kaji Kayastha,** for believing in us, leading us, and inspiring us during the entire project.

Also, we would like to thank the Department of Mechanical and Aerospace Engineering, Institute of Engineering, Pulchowk Campus, for providing us with the opportunity to participate in a collaborative project that has allowed us to apply the knowledge we have gained over the years as a final year project for the final year, which has greatly enhanced our knowledge and broadened our horizon. We'd also like to thank all of our friends who have supported us with this project, both directly and indirectly.

Authors:
Aarati Kunwar
Dikshit Guragai
Manisha Aryal

ABSTRACT

The increasing demand for the use of electric vehicles has created the need for the design of an electric vehicle chassis frame that could sufficiently bear the load of all the components to be fitted into the electric vehicle. This paper presents the chassis frame specially designed for electric vehicles. The Ashby chart is used to select the material, and structural steel is selected after considering different selection criteria. The concepts of solid mechanics are used to select the beam of suitable cross-sectional area. Rectangular hollow section beam is selected over the beam of other cross-sections as it has better performance on vertical bending, lateral bending, and torsional deformations. Maximum bending moment calculation is performed to figure out the minimum sectional modulus for the rectangular hollow section beam. A rectangular hollow section beam with a sectional modulus value of 87.54 mm^3 with dimension 120*80/8 is used for the long side members of the frame, whereas a beam with a sectional modulus of 17.05 mm^3 of dimension 80*40/4 is used for the cross members linking these side members. An iterative method is used to figure out the minimum value of sectional modulus that would effectively handle all the load applied to the chassis frame. The final chassis frame has a factor of safety of 2.6 for failure by yielding criteria with maximum equivalent stress of 93.58 $N * /m^2$.

Modal analysis is performed on the frame to determine the natural frequencies of the frame. It is observed from modal analysis that the natural frequencies don't match with the external excitation frequencies, which makes the frame safe to use. Finally, the value of bending stiffness and torsional stiffness is determined. The bending stiffness is calculated by applying the 1000N load at the centre of the frame in the negative Y-direction and using the deformation obtained, which gives the value of 6.5197 $*10^6$ Nm^2. Similarly, rear and front torsional stiffness are obtained by keeping the front and rear parts fixed and applying loads on free ends. The front and rear torsional stiffness values for the chassis frame are obtained to be 6.50407$*10^5$ Nm/rad and 7.47384$*10^5$ Nm/rad respectively.

Hence, The chassis is successfully designed for static loading conditions and checked for vibrations. Further dynamic loading tests could be performed to figure out the behaviour of the chassis frame.

Contents

List of Figures

List of Tables

ABBREVIATIONS

AC	Alternating Current
AISI	American Iron and Steel Institute
ASTM	American Society for Testing and Materials
BMS	Battery Management System
CAD	Computer Aided Drafting
CAE	Computer Aided Engineering
CAM	Computer Aided Manufacturing
CFD	Computational Fluid Dynamics
CNC	Computerized Numerical Control
DC	Direct Current
EV	Electric Vehicle
FEA	Finite Element Analysis
FEM	Finite Element Method
GIGO	Garbage-in Garbage-out
HEV	Hybrid Electric Vehicle
ICE	Internal Combustion Engine
LCO	Cobalt Oxide
LFP	Lithium Iron Phosphate
LTO	Lithium Titanate
LWB	Long Wheelbase
NCA	Nickel Cobalt Aluminum Oxide

NCM	Nickel Cobalt Manganese Oxide
PDE	Partial Differential Equation
PMSM	Permanent Magnet Synchronous Motor
SLWB	Super Long Wheelbase
SNR	Switched Reluctance Motor
SUV	Sport Utility Vehicle
TVR	Trevor Wilkinson

LIST OF SYMBOLS

τ	Shear stress
σ	Normal stress
M	Moment
δ	Deflection or Deformation
I	Second moment of area
Q	First moment of area
S	Sectional modulus
V	Shear Force
R	Reaction Force
g	Acceleration due to gravity
$C_{v,R}$	Relative cost per unit volume
P	Performance Indices
ρ	Density of material
E	Young's Modulus of Elasticity

Chapter 1: INTRODUCTION

1.1 Background

Due to a gradual increase in fuel prices, growing environmental awareness, and the need to minimize greenhouse gas emissions, electric vehicles have emerged as an appealing alternative to conventional automobiles. Since they are battery-powered, they must be adequately optimized because they perform less well than conventional vehicles. Worldwide businesses have been conducting research and development to create electric automobiles. The weight of the vehicle, how long it takes to charge the power source, as well as the car's mileage is only a few of the variables that might affect the development. Because of the power source weight and other components inside, an electric automobile is heavier than a standard car. As a result, with various components present in the automobile, one of the issues that will develop is the weight that the car's frame must hold.[7]. The chassis plays an important part in providing improved performance. A car's chassis is the supporting framework that provides structural support for the design and operation of the object. The power train and suspension are just a couple of the parts that are housed in the chassis. A vehicle chassis might occasionally be able to resist loads, but it is not intended to be subjected to such loads for an extended period of time, which could result in catastrophic failure. The structure contributes to a large proportion of the development and manufacturing cost, and many different structural choices are available. The best one must be chosen based on cost, volume, method of production, product application, etc. while ensuring acceptable structural performance. Performance evaluation of a vehicle's structure is related to its strength and durability. A design is aimed to achieve sufficient levels of these with as little mass as possible. [10]

1.2 Problem Statement

Electric vehicles are an emerging technology for the achievement of sustainable transportation. With the rise in the popularity of electric vehicles, the need of dedicated chassis for electric vehicle has arisen. With this project, the preliminary step of the design for the Electric Vehicle chassis frame is going to be put forth for the HiAce vehicle

model which could be used in upcoming electric vehicles. To present an efficient design for the electric vehicle chassis considering every design condition and criteria are defined and the design work is carried out.

1.3 Objectives

1.3.1 Major Objectives

- To design and analyze the electric vehicle chassis frame with the help of FEM.

1.3.2 Specific Objectives

- To select the optimum material for the EV chassis out of available material in the market.
- To select the best model based on the design criteria and modify the model if needed.
- To perform the structural analysis and modal analysis on the chassis frame.

1.4 Significance of Project

This project would add significant value to the current market as it is inclining towards the adoption of electric vehicles. The new design for the chassis frame is proposed in this study, which could be used by manufacturers in the upcoming electric Hiace models. In this project, static structural analysis of the chassis frame is done using finite element analysis software, ANSYS. The factor of safety is reasonable, kept around two to give some safety margin for dynamic analysis as well.

1.5 Assumptions and Limitations

In this project, tasks related to the structural analysis of the chassis frame of electric vehicle are carried out. In doing so, several assumptions have been made which are listed below:

1. To simplify the task of design of electric vehicle chassis frame, essential dimensions are selected with reference to Toyota Hiace model.

2. For analytical calculations, which were performed to figure out the value of the sectional modulus of a rectangular hollow section beam, the total load is assumed to be applied over the two long side members of the chassis frame only. This assumption helped us in analyzing the frame as a statically indeterminate beam and determine the minimum sectional modulus value.

3. The four ends of the chassis frame are applied to fixed load boundary conditions in the simulation environment, whereas in reality the frame is lifted by the suspension system and connected to the road using wheels. Fixed support ignored the effect of the suspension system.

4. During simulation only, the effect of vertical loading is considered which is responsible for vertical bending. Thus, the frame is not tested for lateral loading and horizontal lozenging.

5. Effects of impact loads and dynamic loads are not considered.

6. The final assembly of all the components is the chassis frame to give the idea of the location of those components and no calculation is done to model it. It is developed only for visuals.

Similarly, the limitations of the project are enlisted below:

- Due to the lack of resources, the physical construction of the chassis could not possible and the only way of verification is through the comparison of simulation results with the literature review.

Chapter 2: LITERATURE REVIEW

2.1 Chassis History

The history of the chassis is as old as the origin of the first vehicle itself. The first chassis dates back to the late 1800s.[11] Back then, the frame of the vehicle used to be made of a wooden frame. In 1921, the concept of making a floor structure that would carry the weight of seats, body shells, and other weights was introduced. The first actual spaceframe chassis was produced in the 1930s by Buckminster Fuller and William Bushnell Stout.

The main function of the chassis is to support the weight of the vehicle. To do that there is always the optimization between the weight of the chassis and the efficiency of the vehicle. The increased weight decreases the efficiency of the vehicle and vice-versa. Although some other factors affect vehicle performance, this relation between chassis weight and the efficiency of the vehicle always holds. Hence, the design of the precise chassis means the optimization between the safety level of the chassis and its size.[12]

2.2 Chassis Design and Analysis Reviews

In some studies, It has been found that a 10 percent reduction in vehicle weight could increase the energy efficiency of an electric vehicle by 5 to 8 percent.[13] Also, to achieve the optimum weight topology optimization could be applied using the ANSYS topology optimization tool.

There are several differences between traditional IC engine vehicles and electric vehicles. They differ in the components they contain, their operating principles, and the number of services required for vehicle maintenance. From the study, It has been found that the maintenance cost of the electric vehicle can be decreased by 25 percent, which is quite an achievement. [14][15]

Several studies have been carried out to minimize the weight of the vehicle. One of the ways of minimizing the weight of the vehicle is by the use of light material without compromising the safety of the vehicle. The materials like structural steel, aluminium alloy, and carbon fibre are mostly in use to make the chassis for any kind of vehicle. In the study carried out by Nandhakumar et al., it has been found that the replacement of

steel frame with aluminium 6061-T6 and aluminium 7075-T6 the weight reduction of 65.61 percent and 64.33 percent respectively, without any compromise in safety.

The strength analysis of the chassis is done using the Finite Element Method. FEM could be used to find out the critical stress point in the chassis, the maximum deflection of the chassis, and so on. This helps us in figuring out whether the chassis is safe for use or not which helps in reducing accidents at the initial level. FEM could be used to compare the stress points, deflection, and factor of safety of several chassis and figure out the best among them.[16]

T. Kristyadi et al carried out their study to compare the weight of two kinds of ladder chassis of an electric vehicle, which are solid plate beam chassis and perforated plate beam chassis. By comparing the results, the maximum amount of stress for the perforated frame was found to be increased by 25%, the maximum deflection was increased by 20% and the safety factor was decreased by 20% for the solid frame. The weight of the car was decreased by 22.5%, by the use of the perforated frame. Since the safety factor was within safety range, the use of preformed plate beam chassis was recommended.[17]

The chassis frame during vehicle movements experiences situations like lozenging, bending, and torsion. Cross members are important in increasing the torsional stiffness of the frame. Research done at Pune University analyzed cross members of 80 x80mm square section and 80mm outer diameter tubular cross-section of thickness 4mm. The comparison showed the tubular cross section as a better choice for improving torsional stress since the deformation in the front and rear decreased significantly. While the C -shaped members are important in increasing lateral stiffness.

During a case study, stress analysis of a Hyundai Cruz minibus was performed using the finite element method. ABAQUS software was used for carrying out modelling and simulation. Self-weight was considered for static analysis of the chassis frame and Acceleration, Braking, and Road Roughness were considered for dynamic analysis. It was observed that braking caused more stress on the chassis than acceleration.

The important aspects to be considered while designing a chassis are strength, stiffness, ergonomics, weight, and space. Vehicles require a high volume of batteries so the batteries should be evenly distributed and placed low to the ground. The torsional stiffness of a chassis significantly affects the dynamic characteristics, so high torsional stiffness

is desired. The overall mass of the vehicle plays an important role in terms of vehicle range, so the chassis should be lightweight without affecting the strength of the structure.

In one study, FEM stress analysis was used for fatigue life prediction. ABAQUS software was used for simulation and analysis and ASTM Low Alloy steel A710 (C) was taken for study. The primary objective of the study was to find the highly stressed area where Fatigue Failure will start. It was found out the opening area having contact with the bolt experiences high stress.

An experimental approach for the study of the material for the chassis of the electric vehicle was done. The numerical studies were also performed for the chassis alongside the modelling, testing and simulation. A square beam was used for the vehicle frame and the maximum values of stress, deformation and strain were traced. [18] The next study was performed for the electric bus where the analysis was done for the static as well as the transient loading with different materials. It was stated that the steel material channel section along with the stiffener had the best performance. [19]

Vijayan et al. performed a structural analysis of a chassis for different cross-sections and different materials. On comparison between conventional steel and S glass epoxy composite, they found that steel has superior strength to withstand high load and induced low deformation and stress distribution. Widyanto et al. performed a finite element analysis of an electric vehicle chassis for three materials with different thicknesses. The materials used were Grey Cast Iron, AISI 4130 Alloy Steel and AISI A514 Grade B Alloy Steel. On analyzing the simulation result of Von Misses stress and displacement for all the materials, they concluded the model with AISI 4130 Alloy steel with 6 mm in thickness is optimum due to the lowest stress and displacement among all materials and thicknesses.[20]

2.3 Overview of Chassis

A car's chassis is the supporting framework that provides structural support for the design and operation of the object. The power train and suspension are just a couple of the parts that are housed in the chassis.[21] The following items must be chosen to establish a suitable structure:

- The structural type is appropriate for the planned use.
- Correct organization of structural parts to guarantee appropriate load pathways across the vehicle structure with no gaps.
- Appropriate panel and section dimensions, as well as acceptable joint detail design.

Functions of the Chassis frame

- To transport all stationary loads, as well as passenger and freight loads.
- To be able to tolerate torsional vibration generated by vehicle movement.
- To sustain the centrifugal force generated by the vehicle's cornering.
- To resist bending stresses caused by the front axles and rear axles rising and falling.

2.3.1 Ladder type

It is one of the oldest chassis and is called so because the base structure resembles a ladder. It has two heavy and long beams which are supported by two short beams. The ladder chassis' principal advantage was its ease of fabrication and the car assembly. The ladder chassis is fairly substantial, and its strong bending rigidity makes it ideal for transporting heavy items. It's easier to put together because parts can be simply inserted. It does, however, have low torsional stiffness, making it unsuitable for cornering.
Used in: SUVs like Fortuner, Endeavor,etc.

Figure 2.1: Ladder Chassis[1]

2.3.2 Monocoque Chassis

A monocoque chassis is a construction that joins the body and chassis to form an integrated structure in which the vehicle's motion-induced stress is spread throughout the structure rather than forming localized tension. It's made up of multiple sections that have been welded together. In a stream production line, robot arms spot weld the floor pan which is the largest part, and other sections together. After that, extras such as doors, bonnets, side panels, and roofs are added. Because the entire structure is an outside shell, there are no massive high door sills, transmission tunnels, or large roll-over bars, which makes it particularly appealing to mass-market vehicles. It is a low-cost material for mass manufacture. It comes with excellent crash protection and torsional rigidity.

Nearly all mass-production cars adopt this system.

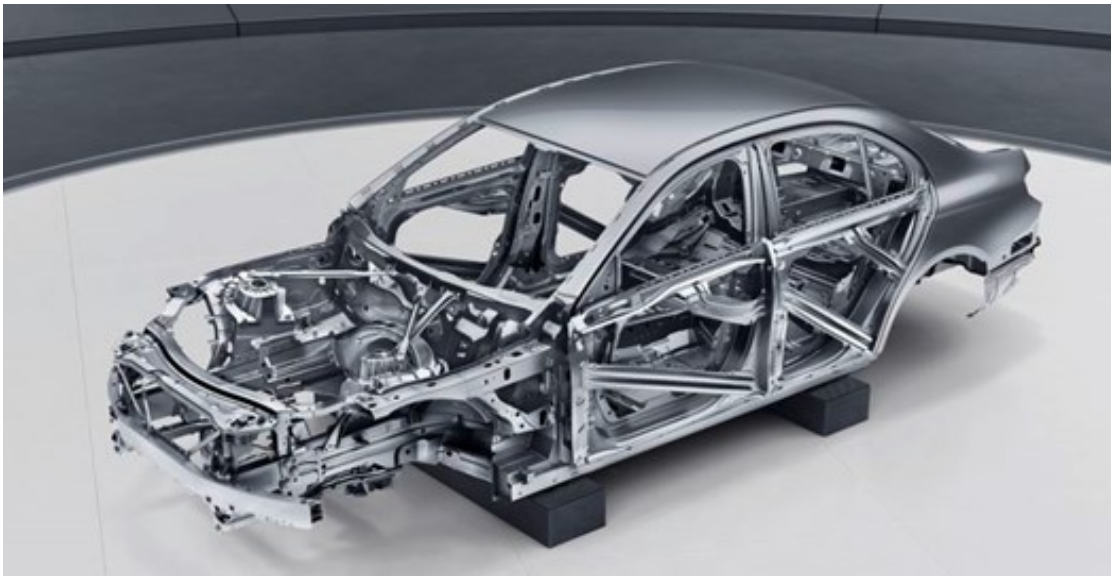

Figure 2.2: Monocoque Chassis [2]

2.3.3 Backbone Chassis

It is a rectangular-section cylindrical tube that joins the front and rear axles and provides practically all of the mechanical strength in the chassis. The body is built on the backbone which is usually made of glass fiber. This type of design is desired when low-volume production is desired.

This type of construction allows for a better connection of the axles to the ground. Because the driveshaft is protected by the chassis, it is far more likely to sustain off-roading, and its high torsional rigidity allows it to withstand more twists. However, it is not suitable for mass production.

Used in: Lotus Esprit, Marcos, TVR, etc.

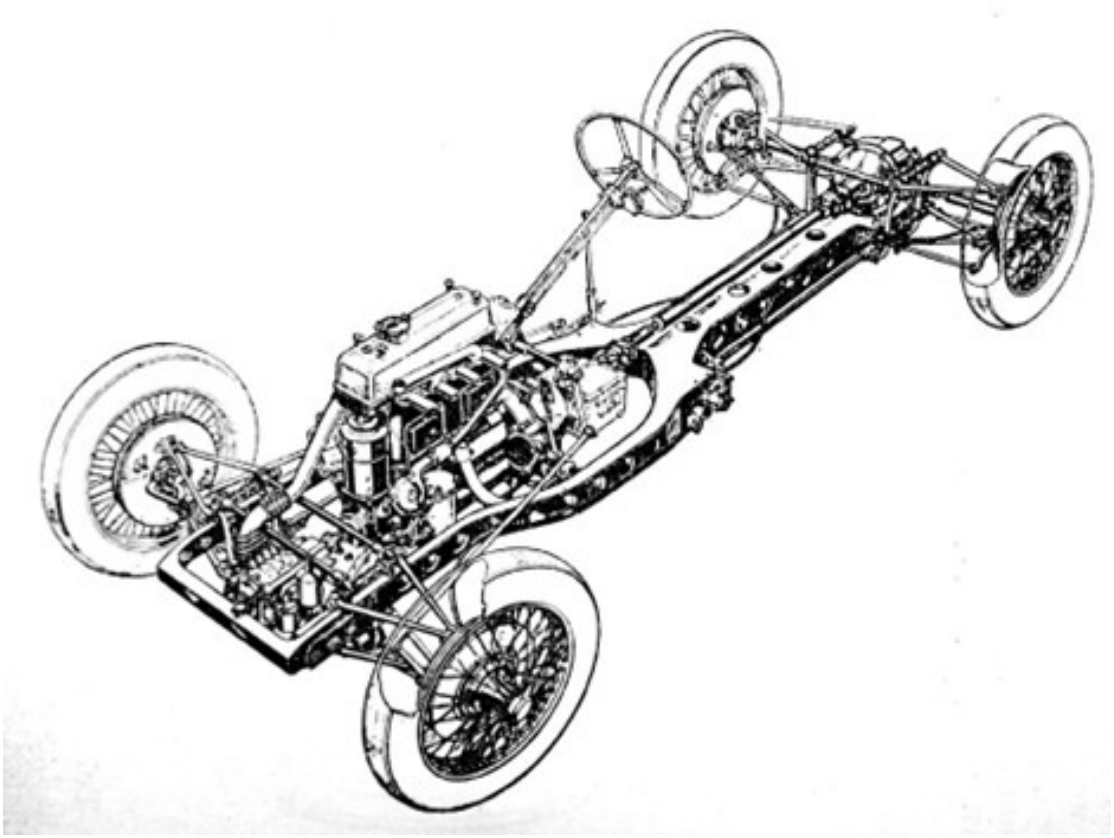

Figure 2.3: Backbone Chassis[3]

2.3.4 Tubular frame

To give mechanical strength against the force applied, this form of chassis uses several numbers of circular cross-section tubes (or square cross-section tubes) in various directions. Welding is done on the tubes to create a complicated structure. Tubular space frame chassis typically feature a robust framework under both doors for the higher strength that is needed by sports vehicles with high performance, resulting in an abnormally high door sill and restricted access to the interior. Tubular chassis are used in race cars due to the superior safety they give. When compared to comparable chassis of the same weight, it is stiffer.

However, because the structure is extremely intricate, expensive, and time-consuming to construct, it cannot be mass-produced.

Used in: All Ferrari before the 360M, Lamborghini Diablo, Jaguar XJ220, TVR, etc.

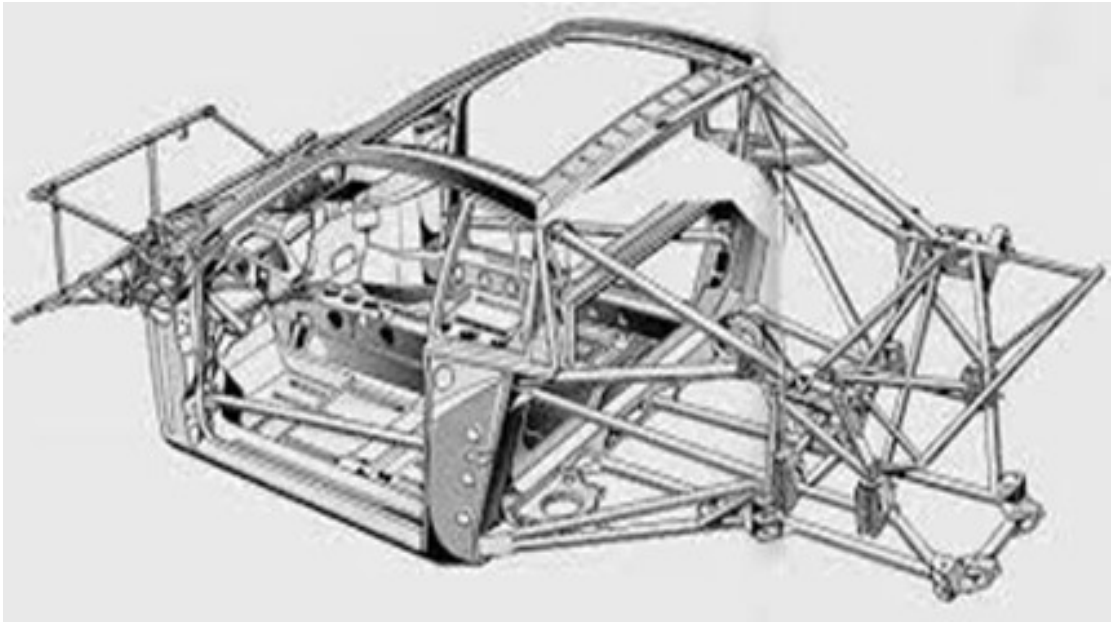

Figure 2.4: Tubular frame [4]

2.3.5 Skateboard Chassis

Automotive platforms for battery electric vehicles are built on a skateboard chassis. The batteries, electric motors, as well as other electronic parts are housed in the base construction. With all components integrated into it, this sort of chassis lowers the cost and simplifies the manufacturing and production complexities. The skateboard's layout can be easily varied by changing the position of the motor. Also depending on the application, the performance can be increased by adding motors to all four wheels.

Figure 2.5: Skateboard Chassis [5]

2.4 Chassis Load

The chassis frame can be considered as a rigid frame as the members have welded connections. The chassis is subjected to different types of loading during stationary and moving conditions of the vehicle. The types of loads on the vehicle chassis can be classified as follows:

- Static Loads: These loads are constant and include the weight of the vehicle, the battery, and the powertrain, as well as the weight of the occupants and any cargo.
- Dynamic Loads: These loads vary with time and include forces caused by the vehicle's motion, such as acceleration, braking, and cornering. Dynamic loads also include the effect of road irregularities and wind resistance.
- Thermal loads: The batteries and powertrain components of an EV generate heat during operation. The chassis must be designed to dissipate this heat and to ensure that the components do not overheat. They give rise to thermal deflection. The chassis of an EV is exposed to thermal loads as a result of the heat generated by the batteries and powertrain components. The chassis can deflect or bend as a result of thermal expansion caused by these loads

- Impact loads: These loads are caused by collisions or accidents and include the forces generated by an impact. The chassis must be designed to protect the occupants and other components in the event of an impact. Transverse deflection occurs when the chassis is subjected to loads that act perpendicular to its length, such as those caused by the forces generated during impact. The chassis can deflect or bend under these loads, causing a deflection in the direction of the chassis.
- Fatigue loads: These loads are caused by the repetitive nature of the loads and the material properties of the chassis. The chassis must be designed to withstand these loads without failing over time. Fatigue deflection could be defined as deflection that occurs when the chassis is subjected to repetitive loads over time. The chassis can suffer from fatigue failure and can deflect or break under these loads.
- Corrosion loads: The chassis of an EV is exposed to different environmental conditions, such as humidity and salt spray, which can cause corrosion. The chassis must be designed to resist corrosion in order to prolong its life.

2.5 Deformation modes of chassis

These loads cause different kinds of deformations on the different members of the frame of the chassis. There are four major modes of deformation of the chassis[22].

- Vertical bending
- Longitudinal torsion
- Lateral bending
- Horizontal lozenging

2.5.1 Vertical bending

Vertical bending is caused during both static and dynamic conditions of the vehicle. This type of deformation is seen in the chassis mostly due to payloads, motor load, battery load, and weight of the vehicle body. The chassis is connected to the wheel through the suspension system which acts as the support. Thus, to prevent the chassis from vertical

bending, the chassis frame must have high bending resistance. High bending resistance of the chassis frame is ensured by the type of structural component used, material properties of the material from which it is made and the transverse load acting on that structure.

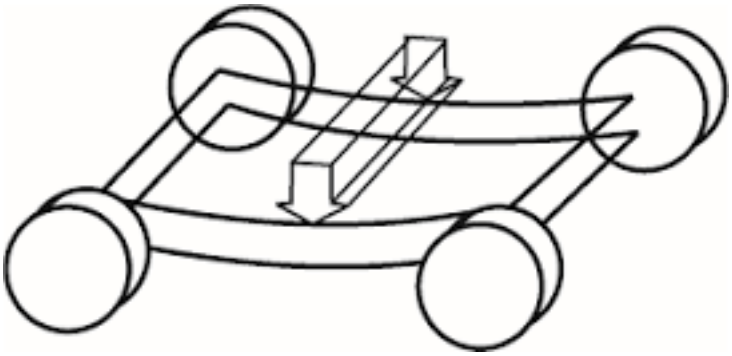

Figure 2.6: Vertical bending[6]

2.5.2 Longitudinal torsion

Longitudinal torsion is the kind of deformation seen on the chassis during the motion of the vehicle on a bumpy road. This is caused when the reaction force of the ground is unequal on the two front wheels or two rear wheels or both. This torsional load affects the vehicle handling and the performance of the vehicle. Thus, the structural members must be strong and stiff enough to handle torsional loading.

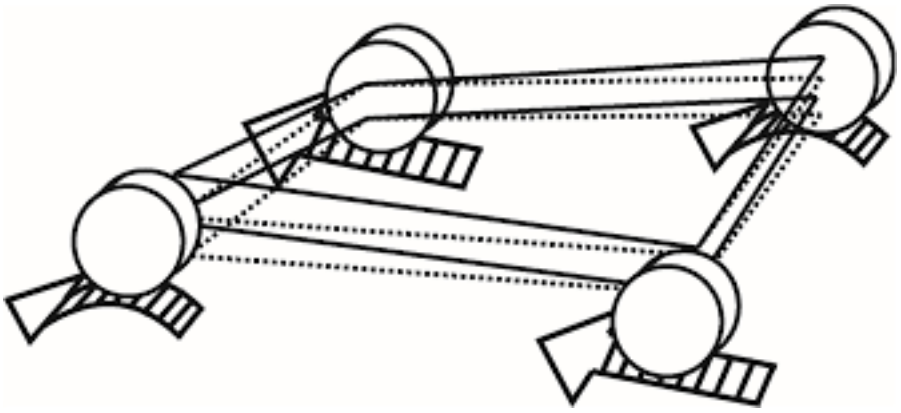

Figure 2.7: Longitudinal torsion [6]

2.5.3 Lateral bending

Lateral bending occurs during the cornering of the vehicle. Load in the lateral direction along with load in the vertical direction causes unsymmetrical bending in the chassis frame. This might cause serious damage to the frame if the frame lacks proper stiffness.

2.6 Toyota HiAce

Toyota Motor Corporation is a Japanese company that handles the production, sales and export of Toyota vehicles.[23] Four different types of HiAce are manufactured by Toyota motor corporation.[24] They are listed below.

- Commuter Widebody (SLWB, High roof)
- Commuter Standard body (LWB, Standard roof)
- Van Standard body (LWB, standard roof)
- Van Widebody (SLWB, high roof)

For this paper, we are designing the chassis for an electric commuter standard body (LWB, standard roof) HiAce. The specifications of the automotive commuter standard body Haice are listed below.

Table 2.1: Basic dimension of chassis

Parameters	Dimension (mm)
Overall length	4695
Overall height	1980
Overall width	1695
Wheelbase	2570
Tread - Front	1470
Tread - Rear	1465
Interior length	3460 (4-row seating)
Interior width	1545
Interior Height	1335
Overhang Front	1050
Overhang Rear	1075

Table 2.2: Weight on the chassis

Parameters	Weight
Curb Weight(kg)	1735-1830
Gross Vehicle Weight (kg)	2750-2950

Table 2.3: Chassis parameters

Parameters	Specifications
Brakes Front	Discs
Brakes Rear	Drums
Suspension Front	Double Wishbone
Suspension Rear	Leaf springs
Steering gear type	Rack and Pinion
Tyres	195R15C

These specifications are used in the current design of the chassis to determine the basic size of the chassis frame.

2.7 Motor

An electric motor is the main component of an EV. Several types of electric motors can now be employed in electric vehicles thanks to the quickly evolving fields of electronics and control systems. High power density, high starting torque, good efficiency, etc., are desirable qualities in electric motors used in automotive applications. Several types of electric motors are used in electric vehicles. They are listed as:

1. DC Series motor
2. Brushless DC motor
3. Permanent Magnet Synchronous motor(PMSM)
4. Three Phase AC induction motors
5. Switched Reluctance motor (SNR)

Comparison of Motors

Table 2.4: Comparison of motors [8]

Parameters	DC series motor	DC Brush-less motor	PMSM	3-phase AC induction motor	SNR
Peak Effi-ciency (%)	85-90	>95	>92	>90	<95
Efficiency at 10% load (%)	80-85	70-80	80-85	>90	>90

Several market trends are also studied while looking at different types of electric motors used in electric vehicles nowadays. Here, the trend of using the PMSM was popularized. It has become the 1st choice for different electric vehicle manufacturers as it provides high torque as well as high power density which is due to the high-energy density permanent magnets used. It had the best mileage performance whereas it has a high cost

compared to motors having the same power. It is hence suitable for high-performance electric vehicles where cost is not a sensitive topic. [25]

2.8 Battery

In an electric vehicle, the battery is one of the most important components which is required to power and propel the electric vehicles. There are several types of batteries for electric vehicles available in the market today. Some of them are listed below:

1. **Lithium-ion Batteries**

   Electric vehicle lithium-ion batteries are the best. If money were no object, a lithium-ion battery would be chosen. Because lithium has the highest electrochemical potential and specific energy of any metal, pound for pound, most lithium batteries, regardless of the cathode material, can be cycled well over a thousand times. Many Lithium-ion battery chemistries were created expressly to be charged by a straightforward controller. Another benefit of adopting lithium-ion batteries is that they require very little maintenance and only a basic battery management system (BMS) to guarantee battery safety and longevity. Lithium-ion batteries come in a variety of forms, so selecting the right one was the first step in analyzing lithium ions. Cobalt Oxide (LCO), Nickel Cobalt Aluminum Oxide (NCA), Nickel Cobalt Manganese Oxide (NCM), Manganese Oxide (LMO), Titanate (LTO), and Iron Phosphate are the six most widely used varieties of lithium-ion batteries (LFP). Lithium-ion batteries get their name from the cathodes, the active components that give the battery its distinct properties. The advantages of each of these several cathode materials for the battery vary.

2. **Lead-Acid Batteries**

   Lead acid batteries are a popular and reasonably priced form of battery. There are specific lead acid battery types that are best suited for use in electric vehicles; nevertheless, not just any lead acid battery would be practical. For instance, a battery used to start an engine in the majority of gasoline-powered cars could not be used in an electric vehicle. Starting batteries can only produce one short

burst of energy before needing to be recharged by the alternator while the vehicle is in motion. A deep-cycle battery is a sort that must be used for every electric car. Deep cycle batteries are created specifically to deliver dependable power for longer periods. The ability of a deep cycle battery to be repeatedly discharged from full capacity to empty is its most significant feature. A deep cycle battery can be entirely emptied several hundred times before the same result is obtained, in contrast to a standard starter battery, which can only be depleted about ten times before losing its capacity to hold a charge. The choice of a deep-cycle lead acid battery can be seen as a workable alternative given that lead acid batteries can power the car.

3. **Nickel-Metal Hydride Batteries**

Nickel-metal hydride batteries, which are frequently used in computers and medical equipment, offer sufficient specific energy and specific power capacities. While safer and more resilient to misuse, nickel-metal hydride batteries have a significantly shorter lifespan than lead-acid batteries. These batteries have been utilized a lot by HEVs. Nickel-metal hydride batteries' high cost, high self-discharge, large heat production at extreme temperatures, and need to control hydrogen loss are its greatest drawbacks.

Comparison of different Lithium-ion batteries

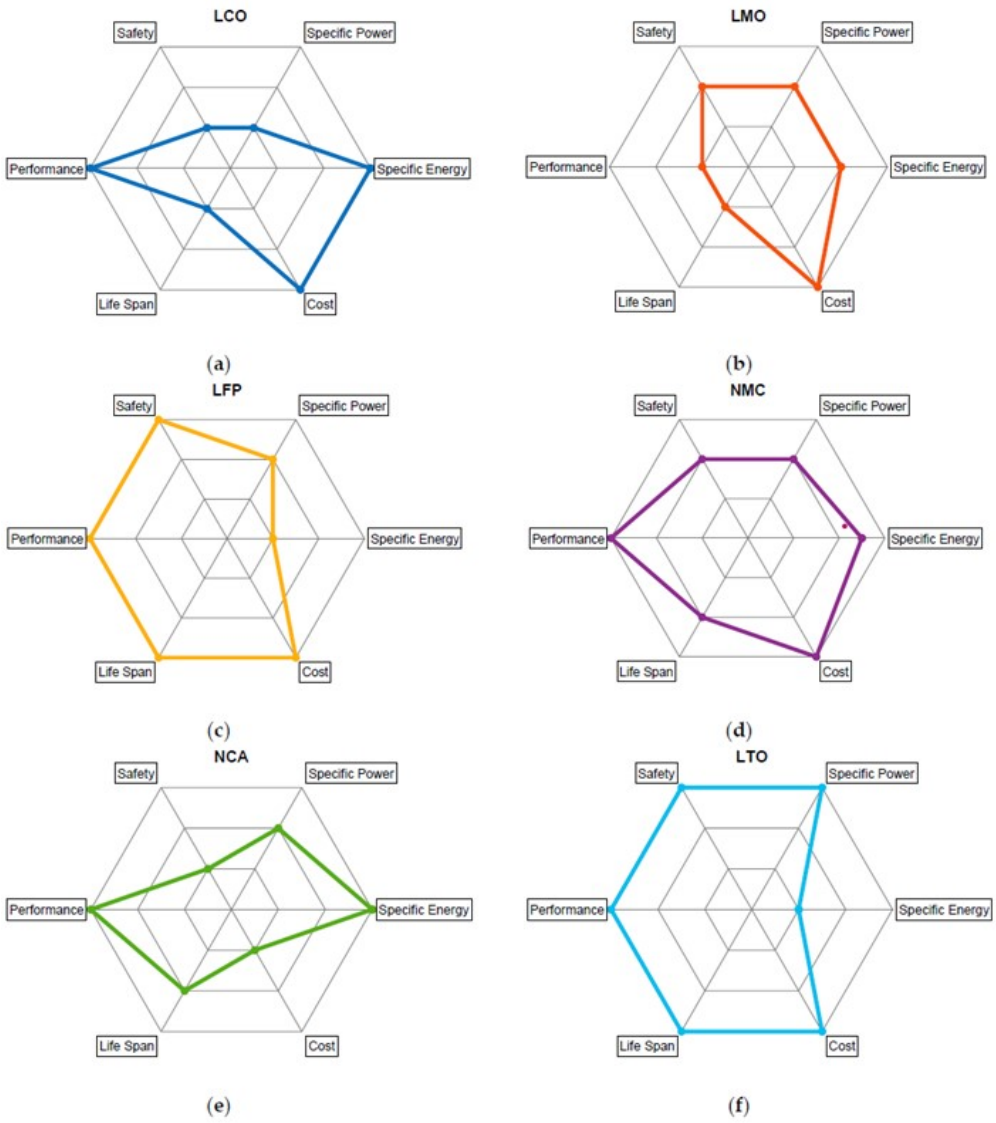

Figure 2.8: Lithium-ion (Li-Ion) technology comparison. (a) LCO; (b) LMO; (c) LFP; (d) NMC; (e) NCA; (f) LTO [7]

LFP battery was developed in 1997 which was able to reduce the cost of the Li-ion batteries which helped in the application in the large-scale commercial. It also offered thermal and cycling stability, improved safety as well as environmental resilience which made it one of the popular choices for electric vehicles battery. [26]

2.9 Design of Prismatic beam

The design procedure of the prismatic beam is as follows:[9]

1. After selecting the material for the beam, list down the values of allowable normal

stress (σ_{all}) and shear stress (τ_{all}). These values could be obtained by dividing ultimate tensile strength and shear strength by the suitable factor of safety.

2. Draw the shear force and bending moment diagram to find out the maximum absolute value of $|V|_{max}$ and $|M|_{max}$.

3. Select the minimum value of section modulus for the obtained $|M|_{max}$ value using the following relation.

$$S_{min} = \frac{|M|_{max}}{\sigma_{all}}$$

4. Among the available beam section, select the one with section modulus,

$$S > S_{min}.$$

5. Now, check for the resistance of the selected beam to the shear stress using the formula given below:

$$\tau_m = \frac{|V|_{max} * Q}{It}$$

6. If $\tau_m > \tau_{all}$, then a stronger beam is selected with a section modulus greater than we previously selected. Otherwise, the beam considered in step 4 is selected.

2.10 Finite Element Method (FEM)

A numerical method for resolving partial differential equations (PDEs) which appear in a variety of engineering and physics applications is the finite element method (FEM). It is an effective tool for modelling the behaviour of intricate structures and systems under various circumstances. The finite element method's fundamental principle is to divide a complex domain into a finite quantity of simpler, smaller subdomains or elements for approximation of the solution to PDE over that domain. At certain locations known as nodes, these subdomains are joined to create a mesh. A collection of polynomial basis functions are then used to estimate the solution over each element,

and the results are merged to produce an overall approximation of the solution over the whole domain. Many engineering and science issues, including fluid dynamics, structural analysis, electromagnetic fields, heat transport, and many others, can be solved using the finite element approach. For issues that are too time-consuming or complex to be resolved analytically or with other numerical techniques, it offers precise and effective solutions.

The following matrix equation denotes the Finite Element equation:

$$[K]\{u\}=\{F\}$$

where

[K]=Global Stiffness Matrix

{u}= Nodal Displacement

{F}= Nodal force

2.10.1 ANSYS

John Swanson started ANSYS in 1970, and it is reported that the company was sold to venture capitalists in 1993. High scalability and extensive Multiphysics product modelling solutions are offered by ANSYS. The analysis is carried out by Ansys using the finite element method. To accomplish the solutions based on various numbers of nodes as requested by the analyzer or designer, FEM was developed. FEM uses many sorts of matrices to represent the required item under study's geometry, load, material properties, temperature, stiffness, etc. The number of nodes chosen for analysis and the order of the matrix utilized in FEM equations are the same. As a result, FEM is an approximation of the same analysis that was produced from the mathematical model; however, in this instance, the parameters are set in accordance with the elastic analogy of the material matrix, which illustrates the same characteristics as anticipated in the mathematical model. ANSYS is renowned for its adaptability. As ANSYS already includes CAD modelling tools, importing a model from another CAD program is also suitable for analysis. In particular, ANSYS provides an analysis platform for structural analysis, thermal analysis, and CFD issues.

2.10.2 Element Quality

The quality of the mesh is an essential factor in determining whether the results generated are trustworthy or not. There are several metrics to check mesh quality such as Jacobian ratio, orthogonality and skewness. The Jacobian ratio of elements lies between 0 and 1 and the more it is to 1, the better the mesh is considered. Similarly, orthogonality also lies between 0 and 1 and similar to the Jacobian ratio good quality mesh has orthogonality near to 1. Mesh is considered better if it has maximum skewness of less than 0.95 and an average below 0.33.[27]

2.11 SOLIDWORKS

Dassault Systems created SOLIDWORKS with the primary goal of solid modelling with CAD and CAE-based designs. Despite the fact that no information is provided by developers regarding the operating system of software, SOLIDWORKS is primarily run on Windows. Because of its user-friendly interfaces for building reliable models, SOLIDWORKS is most frequently used to execute the CAD modelling of complex components. The model built in SOLIDWORKS can be exported to simulation software such as ANSYS, CATIA, and many more; or it can be made directly by loading the file on CNC manufacturing CAM software such as Creo. SOLIDWORKS' popularity is a result of how simple it is to create 3D models with it and how easily components can be put together quickly.

2.12 Ashby charts

There are several materials, and each one has numerous characteristics. It requires a suitable method to present and contrast them. Plotting these parameters as Material Property Plots, also known as bubble/ Ashby charts, including 1 property on 1 axis and then another characteristic on the other, is an effective way to accomplish this. Depending on the precise composition, heat treatment, grade, supplier, etc., every material has a variety of values for every property. The value range of the attributes determines the width and height of the ellipses or bubbles that depict the materials on the chart. The axes range on the charts is selected to cover all materials, from light as well as flexible polymer foams to dense, stiff, and strong metals like tungsten. The use of logarithmic

scales, where each significant step on the axes reflects a factor of 10, allows for the coverage of this vast range. There are numerous applications for these charts. They may be employed to choose materials for new models or to replace materials in a product that is already in demand. They can be applied to data comparison and estimation. Additionally, they can be used to visually discover trends in characteristics, including how processing impacts properties and the connections between them. Some of the examples of the Ashby chart are young's modulus VS Density chart, Strength VS Density chart, Strength VS Relative cost per unit volume chart and so on. The modulus density chart by Ashby is shown below which shows us several materials comparisons for Young's modulus and density. This chart helps us to determine the modulus of different engineering materials and compare them with the density to get the required yield strength in the material.

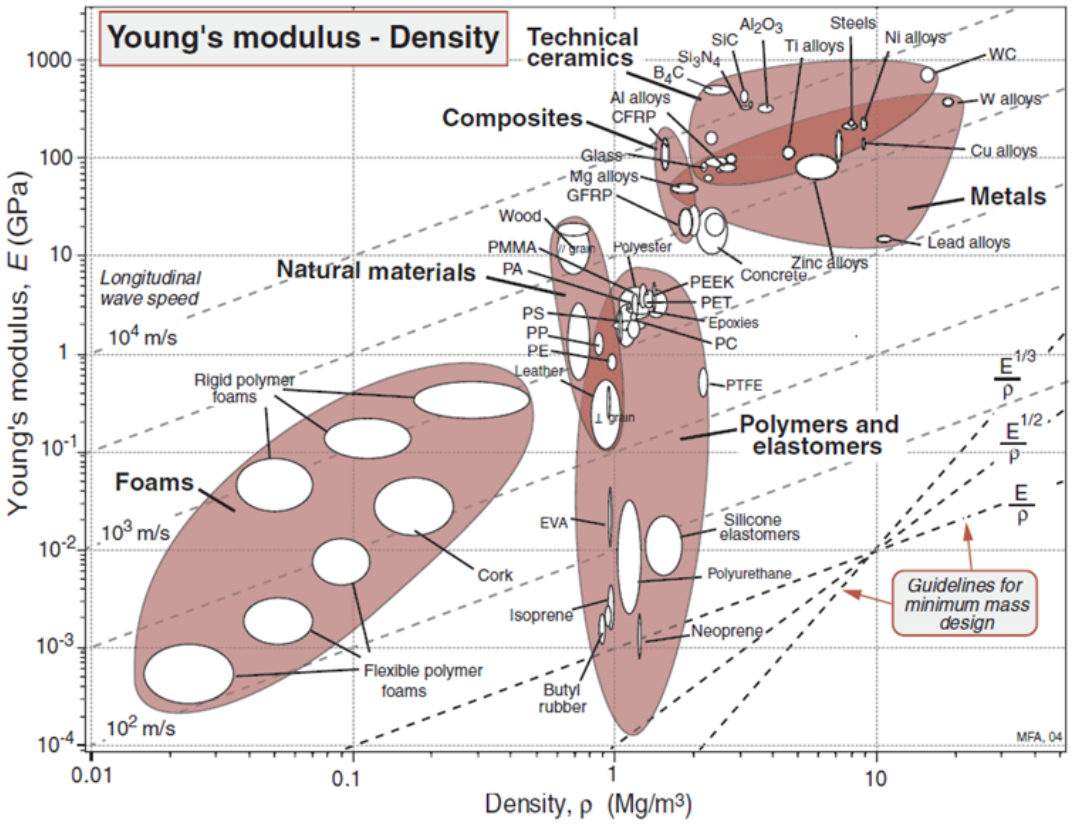

Figure 2.9: Young's modulus-Density Chart for different materials

[28]

The above chart shows the contrast between the strength and density of different engineering materials. This chart can be used to determine the required properties of the

material. The Strength-relative cost per unit volume chart by Ashby is shown below which shows us several materials comparisons for the strength and relative cost per unit volume chart. This chart helps us to determine the strength of different engineering materials and compare them with the cost to get the balance between the required strength and cost.

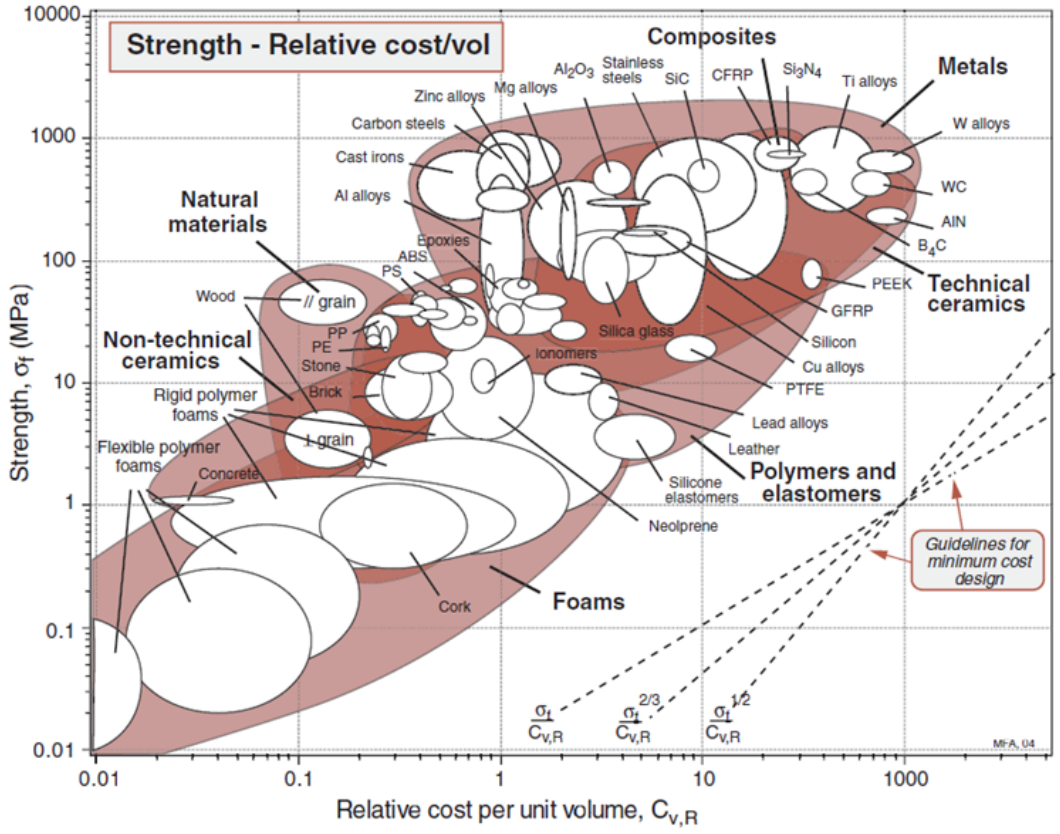

Figure 2.10: Strength-relative cost per unit volume chart for different materials [28]

The above chart shows the chart for the strength-relative cost per unit volume chart by Ashby.

Chapter 3: METHODOLOGY

The following methodology is followed in this project.

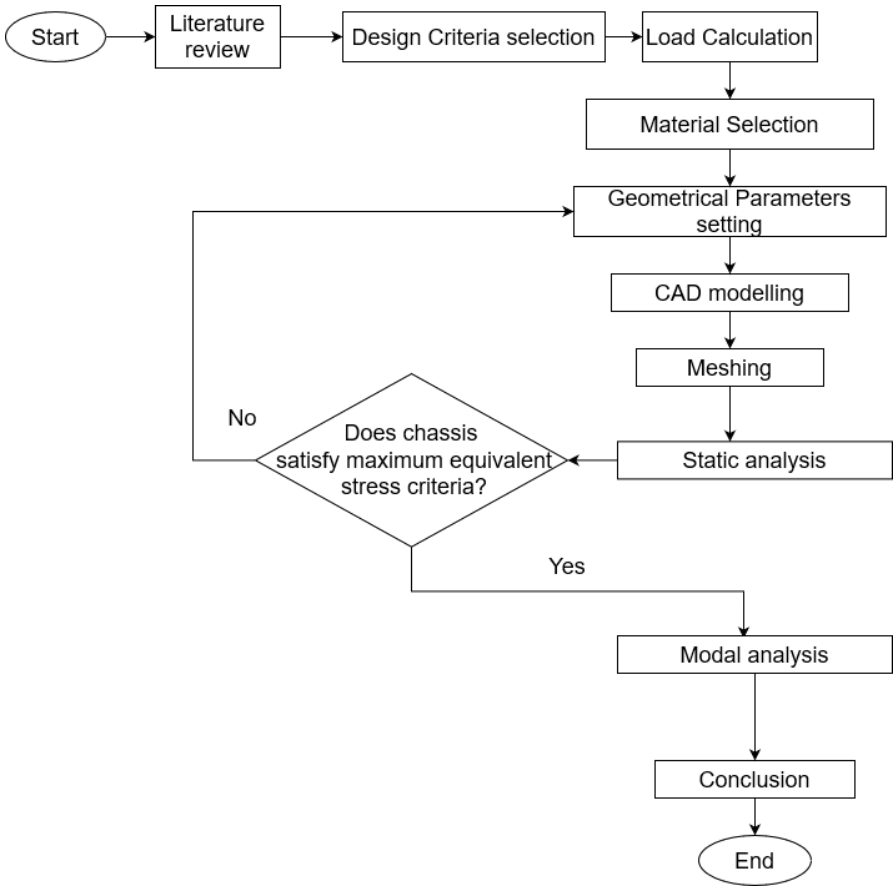

Figure 3.1: Methodology Chart

The project started with a Literature review to figure out the research gap and the task of Literature review continued throughout the project. Design selection criteria are done with the help of a Literature review. Load calculation is done with reference to the Toyota Hiace vehicle and on the basis of this load calculation, material and component selection is done.

The battery and motor selection process, material selection process, CAD modelling of the chassis frame and simulation process all are explained below in detail.

3.1 Chassis type selection

Different types of chassis for vehicles were explored and it was found that the chassis that was suitable for the chosen HiAce (minibus) was the ladder chassis. The frame for the ladder chassis used 2 side members which were joined with different series of cross members that were placed at high-stress points. It helped in the minimization of deflection as well as the mass of the chassis frame. Hence, the ladder chassis was chosen for the design of the electric HiAce. [29]

3.2 Motor and Battery Selection

With the study of the present trends of the motors used in different electric minibuses, it is assumed that the 90kW motor is sufficient for our desired design of the chassis for the Toyota HiAce. The following motor is chosen for the load consideration in our design. For battery as well, as the battery rating available nowadays ranged from 40kWh to 100kWh, it is assumed that the battery rating is 79kWh for our vehicle.

Table 3.1: Motor specifications

Particulars	Values/Specifications
Manufacturer	Rawsun Power Co. Limited
Motor type	Permanent magnet synchronous motor
Peak Power	130kW
Rated Power	90kW
Peak torque	500Nm
Rated torque	285Nm
Peak speed	4500rpm
Rated speed	3000rpm
Peak current	300A
Rated current	170A
Mass	87kg

Battery weight calculation:

Energy density=140Wh/kg [30]

Battery rating of 79kWh is assumed,
Mass=79000/140=564.28 kg

3.3 Material Selection

Material selection is the key step in the mechanical design process. This is a crucial step as it affects the overall weight, size, and ability to withstand the load of the mechanical components. Several parameters are considered before selecting the material for the project. The selection criterion of material is different for a different project. Material to fabricate the chassis is selected based on the physical and mechanical properties of the material, reliability, durability, cost, weight, recyclability, yield resistance, and corrosion.

3.3.1 Performance Index

A performance index is a constant that is defined for selecting the best-performing material for a particular case. In this study, four performance indices are defined for the minimization of the mass and cost as well as to choose the best material for the chassis elements.

Here,

$$\text{Performance index(P)}\alpha\ \frac{1}{m}\ \text{(Mass Minimization)}$$
$$\text{Performance index(P)}\alpha\ \frac{1}{C_v,R}\text{(Cost Minimization)}$$

Let us consider 2 cases:

1. **Beam undergoing bending:**

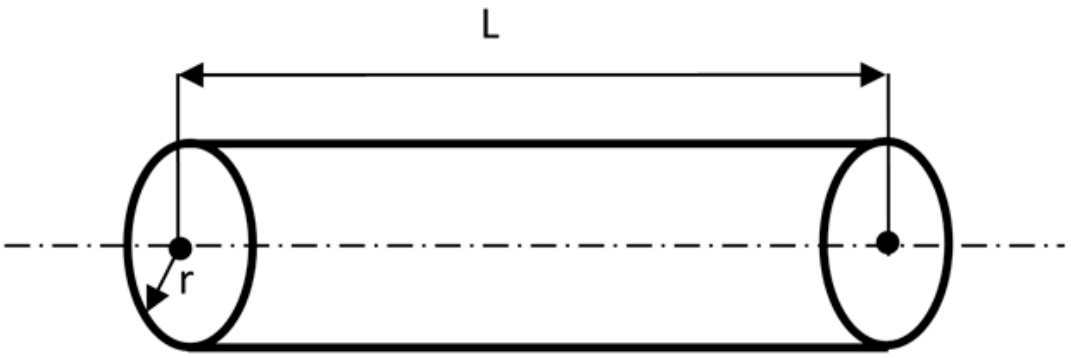

Figure 3.2: Circular Cross-section beam

$$\text{Deflection}(d) = \frac{WL^3}{48EI} \tag{3.1}$$

Here,

d= Deflection

L= Length of beam frame

I= Second moment of Area around the Neutral axis

W= Weight in frame

E= Young's Modulus

For circular beams,

We have, mass(m) = $\pi\ r^2 \mathrm{L}\rho$

Here,

R=Radius of cross-section

ρ=Density of the beam material

$$r = \sqrt{\frac{m}{\pi \mathrm{L}\rho}} \tag{3.2}$$

And

$$I = \frac{\pi r^4}{4} \tag{3.3}$$

Solving (5.1) and (5.3)

$$d = \frac{WL^3}{48E(\frac{\pi r^4}{4})}$$

$$\text{Or,} d = \frac{WL^5\pi\rho^2}{12Em^2}$$

$$\text{Or,} m = \left(\frac{WL^5\pi}{12d}\right)^{1/2}\left(\frac{\rho}{\sqrt{E}}\right)$$

Here, the first term of the equation i.e. $\left(\frac{\text{W}pi}{12d}\right)^{1/2}$ is the properties of the the beam that is dependent upon the loading parameter and the geometry.

The second term for the equation i.e. $\left(\frac{\rho}{\sqrt{E}}\right)$ is dependent on the material properties and also can be called material index.

For the performance index,

P_1 can be defined as the first performance index which is the reciprocal of the material index.

Here,

$$P_1 \propto \frac{\sqrt{E}}{\rho} \tag{3.4}$$

2. **Beam undergoing axial loading:**

$$Deflection(d) = \frac{WL^2}{\text{AE}} \tag{3.5}$$

Here,

d= Deflection

L= Length of beam frame

A= Area of cross-section

W= Weight in frame

E= Young's Modulus

For circular beams,

We have, mass$(m) = A\text{L}\rho$

Where,

ρ=Density of the beam material

$$A = \frac{m}{\mathrm{L}\rho} \tag{3.6}$$

Solving (5.5) and (5.6),

$$d = \frac{WL^2}{\frac{m}{\mathrm{L}\rho} * E}$$

$$d = \frac{WL^3}{\frac{E}{\rho} * m}$$

$$m = \frac{WL^3}{d} * \frac{\rho}{E}$$

Here, the first term of the equation i.e. $\frac{WL^3}{d}$is the properties of the beam that is dependent upon the loading parameter and the geometry.

The second term for the equation i.e. $\frac{\rho}{E}$is dependent on the material properties and also can be called material index.

For the performance index,

P_2 can be defined as the first performance index which is the reciprocal of the material index.

Here,

$$P_2 \propto \frac{E}{\rho} \tag{3.7}$$

From the definition of the performance indices P_1 and P_2, We have,

$$P_1 \propto \frac{\sqrt{E}}{\rho}$$

Or, $P_1 = \frac{\sqrt{E}}{\rho} * C_1$

Where C_1 is the proportionality constant,

Taking logs on both sides,

$$\log(P_1) = \frac{1}{2}\log(E) - \log(\rho) + \log(C_1)$$

Or,

$$\log(E) = 2\log(\rho) + 2\{\log(P_1) - \log(C_1)\} \tag{3.8}$$

Also,

$$P_2 \propto \frac{E}{\rho}$$

And $P_2 = \frac{E}{\rho} * C_2$

Taking logs on both sides and solving,

$$\log(E) = \log(\rho) + \{\log(P_2) - \log(C_2)\} \tag{3.9}$$

As the obtained equations (3.8) and (3.9) are in form of a linear equation i.e., in the form of y=mx+C, two linear lines can be traced in the modulus versus density plot while taking the significant value of the performance index as shown below. Plotting the equations (3.8) and (3.9) in the Ashby chart of Young's modulus-Density, we get,

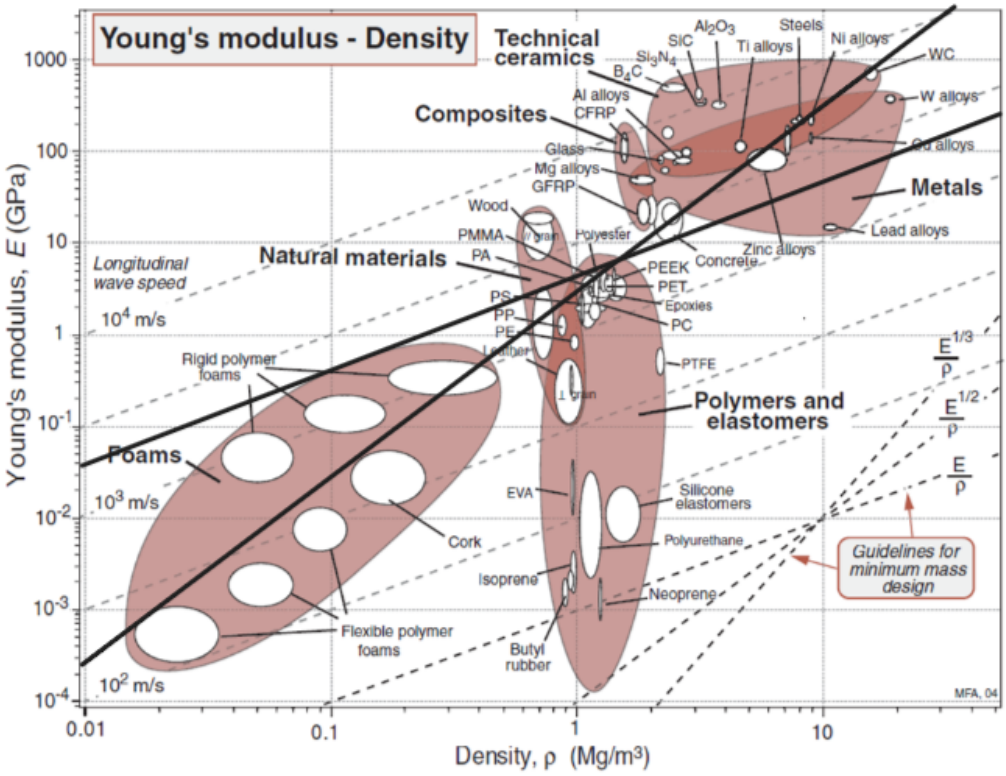

Figure 3.3: Young's Modulus-Density Chart depicting minimum mass design lines [28]

Here, two lines can be observed intersecting and the materials included by both lines and remaining on the upper zone are required for the electric chassis material. From the above graph, the following materials are enlisted as the first choices of material.

Table 3.2: Shortlisted materials using P_2 and P_2 performance indices

SN	List of Materials	Young's Modulus (E) in GPa	Density (ρ) in kg/m^3	$\frac{E}{\rho}$	$\frac{\sqrt{E}}{\rho}$
1.	Aluminium Alloy	80	2500	0.032	0.0038
2.	CFRP	110	1600	0.069	0.0066
3.	Steels	220	8000	0.028	0.0015
4.	Titanium alloy	110	4200	0.026	0.0025
5.	Magnesium Alloys	40	1900	0.021	0.0033
6.	Cast Iron	95	7130	0.0133	0.0013

Let us define two different performance indices for the optimization of the cost as well.

Performance index(P_3)= $\frac{\sqrt{\sigma}}{C_{v,R}}$ (for bending load)

Performance index(P_4)= $\frac{\sigma}{C_{v,R}}$ (for axial load)

Plotting the respective plots from the above equation in the Ashby chart of Strength-Relative cost,

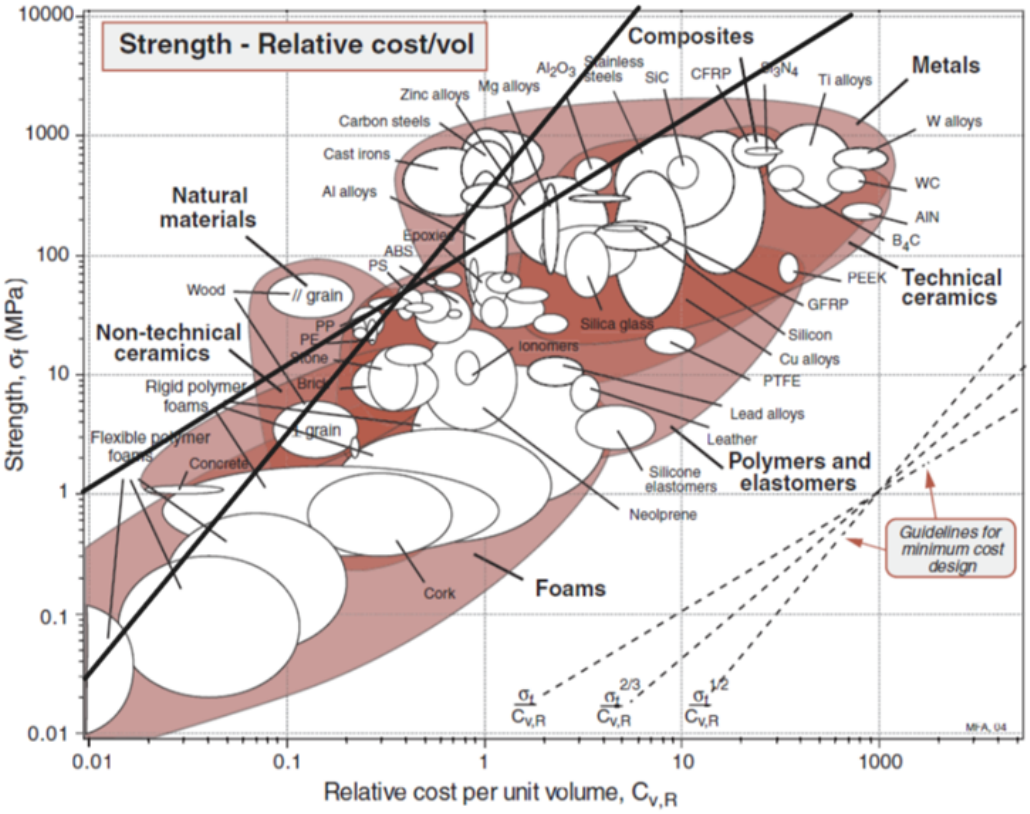

Figure 3.4: Strength-relative cost per unit volume chart depicting minimum cost lines [28]

Here, the enlisted materials using performance indices P3 and P4 are as follows:

Table 3.3: Shortlisted materials using P_3 and P_4 performance indices

SN	List of Materials	Strength	Relative Cost per unit volume ($C_{v,R}$)	$\frac{\sigma}{C_{v,R}}$	$\frac{\sqrt{\sigma}}{C_{v,R}}$
1.	Aluminium Alloy	200	1.2	166.667	11.785
2.	Cast iron	350	0.9	388.889	20.78
3.	Carbon Steels	550	1	550	23.452

3.3.2 Material selection matrix

After shortlisting and filtering out material using both Ashby's charts, the selection of the material is done with the material selection matrix. Here, weightage is assigned to different parameters of material qualities and points are assigned to the material on the basis of those parameters. the weightage is summed up to a total of "1" and the point that could be assigned to the materials were in the range of 100 to 400 respectively.

Table 3.4: Material Selection Matrix

Material Qualities		Carbon Steel		Cast Iron		Aluminium Alloy	
Parameters	Weightage	Point	Total	Point	Total	Point	Total
Durability	.25	100	25	300	75	200	50
Availability	.25	400	100	300	75	200	50
Manufacturability	.25	400	100	200	50	300	75
Flexibility	.2	400	80	200	40	300	60
Aesthetics	.5	100	5	300	15	200	10
Total	1		310		255		245

Here, it can be seen that carbon steel had the highest point which made it the optimum choice of material considering different parameters. It is decided to use structural steel in general as it is one of the popular and sustainable materials of choice for different engineers. ASTM A-36 structural steel has low cost and several applications in the construction of heavy equipment, automotive and so on. Hence, it is chosen to design the chassis of the electric vehicle. [31] Also, it was understood that the ASTM A36 was one of the popular materials used for the chassis building due to its material properties such as temperature resistance, duration along with improvement in lightness, strength and stiffness. [32]Here, the properties of the structural steel ASTM A-36 is listed below:

Table 3.5: Properties of Structural steel A-36 [9]

Properties	Value	Unit
Ultimate Strength (Tension)	400	MPa
Yield Strength (Tension)	250	MPa
Modulus of Elasticity	200	GPa
Modulus of Rigidity	77	GPa
Coefficient of Thermal Expansion	11.7	$10^{-6}/^{0}$C
Ductility Percent Elongation in 50mm	23	%

3.4 Chassis frame Section

Different types of frame sections are available in the market such as I-section, circular section and so on. The properties of all the cross-sections are studied and finally, the rectangular hollow section is selected as it is good for both torsion bending conditions. For all the chassis frame section options, the rectangular box section can offer maximum bending stiffness relative to its weight and also the rectangular box section has one of the best torsional resistance, making it a suitable choice for the chassis frame section. [33]Also, to back that up, from the evaluation of different cross-sections in a paper review that included a C-section, I-section and box section, it was seen that the box section had the least stress and deformation development in the same chassis design models. [34]

3.5 Load intensity

The loads that act on the frame include battery packs, electric motor, frame weight, passenger loads, cab and different systems. The weight of the chassis is applied vertically downwards along the y-axis with $g = 9.8m/s^2$. According to the study conducted by Baral, et al., the weight of the average Nepalese citizen is 57 kg [35]. The passenger loading at full capacity along with the payload is 11400N for 20 passengers. The passenger load, battery packs, cab and different systems are applied as uniform load along the negative y-axis. Similarly, the weight of the electric motor and the electronic control system is taken as a point load along the Y-axis. The mass of the vehicle body is taken

as 315 kg, and the electronic control system is 80 kg.[15]

The different loads and the loading patterns are tabulated below:

Table 3.6: Loads and their loading patterns

Load type	Weight (N)	Loading
Frame weight	Not considered at this part	Gravity field
Battery	5643	Uniform load
Electric Motor	870	Point load
Electronic Control System	800	Point load
Passenger load	11400	Uniform load
Vehicle body weight	3150	Uniform load
Others	4000	Uniform load

3.6 Calculation

The chassis frame is a complex structure as it involves beam members of different cross-sections which are connected using bolts, rivets or welds. It can be a tedious task to analyze the whole frame at once. Under full-load bending conditions, each member of the frame undergoes bending due to the applied transverse loading. In this situation, each member of the frame can be treated as the beam member undergoing bending. The maximum load-bearing members in this situation are the long side members and the total load uniform acted upon the frame could be distributed between the two side beams and the maximum bending moment in each beam could be obtained easily.[15] The loading condition on each side member is shown in the figure below.

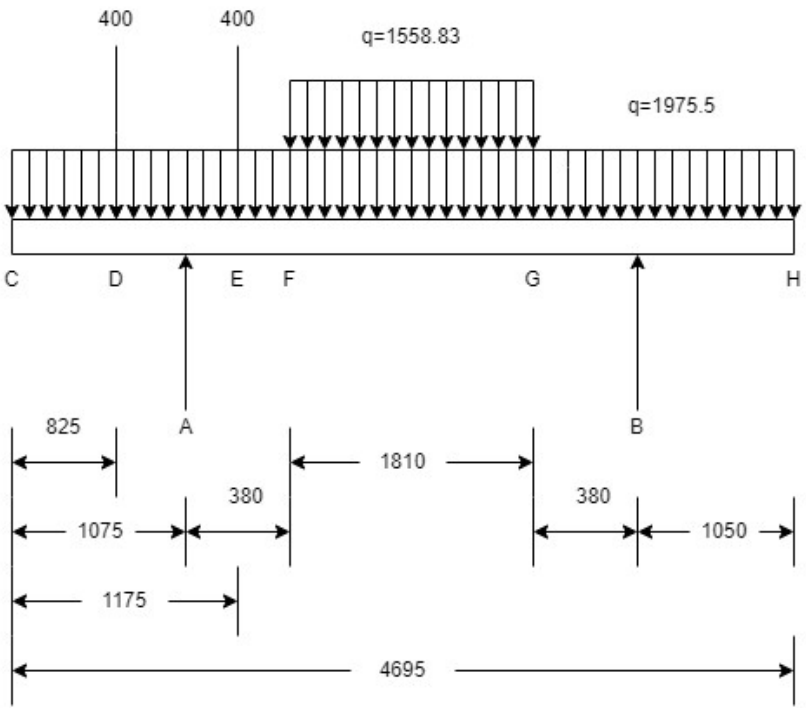

Figure 3.5: Free body diagram of an overhanging beam

Calculation for Reaction force

Here,

$$R_A+R_B=400+400+1559\times1.810+1975.5\times4.695=12896.76\text{N}$$

At A,

$$-400\times0.25+400\times0.1+1559\times1.810\times1.285+1976\times4.695\times1.2725=R_B\times2.570$$

$$\because R_B=\frac{15371.38}{2.570}=5981.08N$$

Then,

$$R_A=6915.67N$$

Calculation for shear force diagram,

$$V_C = 0$$

$V_{\text{CD}} = -1976x \quad \mathbf{V}_{\text{Dleft}} = -1630.2 \quad V_{\text{Dright}} = -2030.2$

$V_{\text{DA}} = -1976(x - 0.825) - 2030.2 \quad V_{\text{Aleft}} = -2524.2 \quad V_{\text{Aright}} = 4391.4x$

$V_{\text{AE}} = 4391.47 - 1976(x - 1.075) \quad V_{\text{Eleft}} = 4193.87 \quad V_{\text{Eright}} = 3793.87$

$V_{\text{EF}} = 3793.87 - 1976(x - 1.175) \quad V_{\text{Fleft}} = V_{\text{Fright}} = 3240.59$

$V_{\text{FG}} = 3240.59 - (1976 + 1558.83)(x - 1.455) = -3157.76 \quad V_{\text{Gleft}} = V_{\text{Gright}}$

$V_{\text{GB}} = -3157.76 - 1976(x - 3.265) \quad V_{\text{Bleft}} = -3908.64 \quad V_{\text{Bright}} = 2072.44$

$V_{\text{BH}} = 2871.85 - 1976 \times (x - 3.645) \quad V_{\text{Hleft}} = 0 \; V_{\text{Hright}} = 0$

Calculation for Bending moment

$M_{\text{CD}} = -1976\frac{x^2}{2} \;\; M_D = -\frac{1976}{2} \times 0.825^2 = -672.46$

$M_{\text{DA}} = -1976\frac{x^2}{2} - 400(x - 0.825) \;\; M_A = -1241.75$

$$M_{\text{AE}} = -1976\frac{x^2}{2} - 400(x - 0.825) + 6915.67(x - 1.075); \; \mathbf{M}_E = -812.49$$

$M_{\text{EF}} = -988x^2 - 400(x - 0.825) + 6915.67(x - 1.075) - 400(x - 1.175); \; M_F = 171.93 \approx 172.33$

$$M_{\text{FG}} = -988x^2 - 400(x - 0.825) + 6915.67(x - 1.075) - 400(x - 1.175) - \frac{1559}{2} \times (x - 1.455)^2$$

$$M_G = 247.29$$

$$M_{\text{GB}} = -988x^2 - 400(x - 0.825) + 6915.67(x - 1.075) - 400(x - 1.175)$$

$$-1559 \times 1.810 \times (\tfrac{1.810}{2} + x - 3.265)$$

$$M_B = -1095.32$$

$$M_{\text{BH}} = -988x^2 - 400(x - 0.825) + 6915.67(x - 1.075) - 400(x - 1.175)$$

$$-1559 \times 1.810 \times (\frac{1.810}{2} + x - \ 2.360) + 5981.08 \times (x - 3.645)$$

$$M_H = 0$$

Using Matlab code for finding out the bending moment and shear force diagram [36], we have

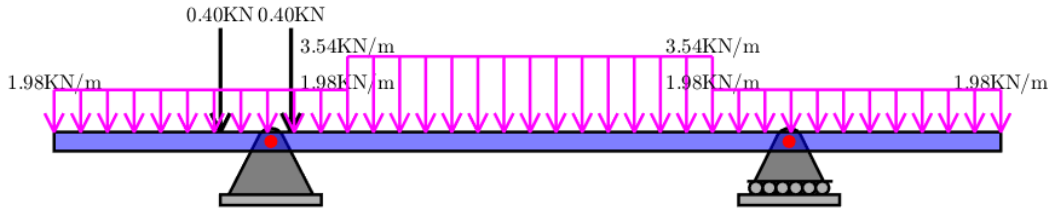

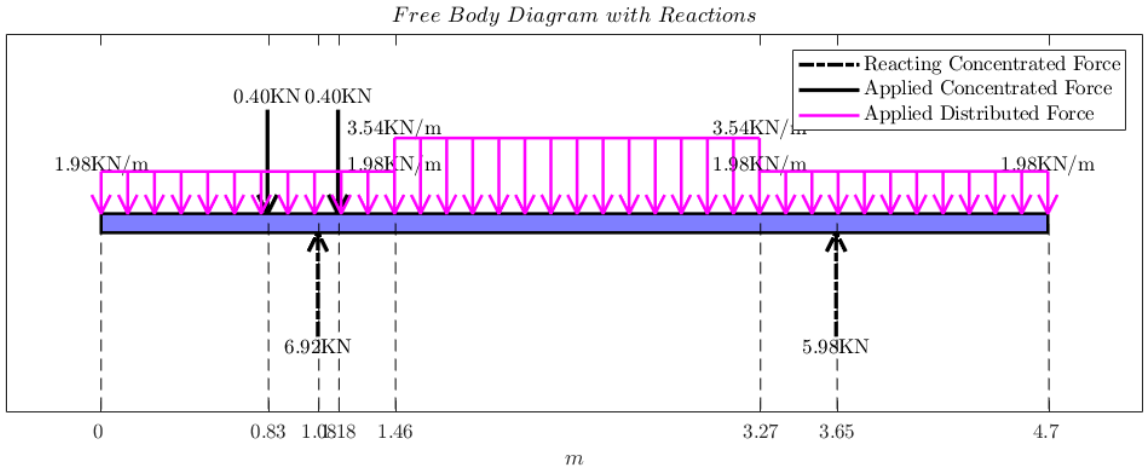

Range	*Equations of Shear Force* :	*Equations of Bending Moment* :
0 *to* 0.825	$-1.975x$	$-0.987x^2$
0.825 *to* 1.075	$-1.975x - 0.4$	$-0.987x^2 - 0.4x + 0.33$
1.075 *to* 1.175	$-1.975x + 6.516$	$-0.987x^2 + 6.516x - 7.105$
1.175 *to* 1.455	$-1.975x + 6.116$	$-0.988x^2 + 6.116x - 6.635$
1.455 *to* 3.265	$-3.535x + 8.386$	$-1.767x^2 + 8.386x - 8.286$
3.265 *to* 3.645	$-1.976x + 3.296$	$-0.988x^2 + 3.296x + 0.024$
3.645 *to* 4.695	$-1.976x + 9.277$	$-0.988x^2 + 9.277x - 21.776$

Figure 3.6: Free body diagram

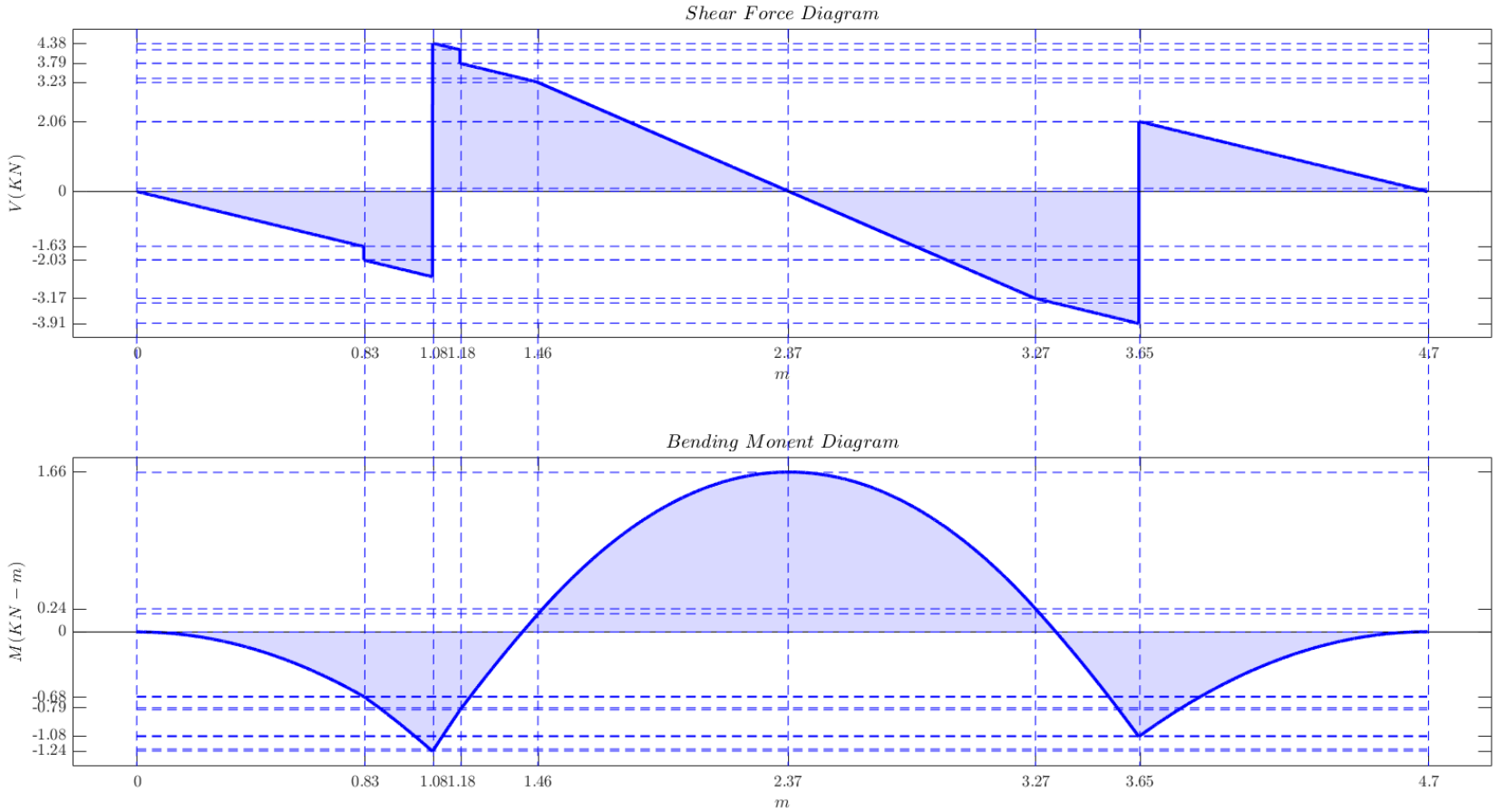

Figure 3.7: Bending moment and Shear force diagram

Now,

$$M_{max} = 1660Nm$$

$$|V|_{\text{max}} = 4391$$

$$\tau_{\text{all}} = \frac{|V|Q}{\text{It}}$$

where, Q=first moment of area

For structural stress,

$$\tau_{\text{all}} = 145MPa$$

$$\sigma_{\text{all}} = 250MPa$$

$S_{min} = \frac{1660}{250\times10^6} = 6.64 \times 10^3\text{mm}^3$

Hence, the selected beam is of sectional modulus,

$$S_{\text{min}} = 7.486 \times 10^3\text{mm}^3$$

$$I_y = 0.1871 \times 10^6\text{mm}^4$$

3.7 Dimension of the chassis frame

The fundamental dimensions for the current chassis frame are taken with reference to the dimensions of the Toyota LWB, standard roof Hiace. The length of the frame is taken the same as the overall length of the vehicle but the width is taken smaller than the overall width of the vehicle. The width is taken by allowing space for the tyres and suspension system. Since the section width of the chassis is 195mm. [37]

Distance between the inner side of the front or rear tyres = $1695 - 195 * 2 = 1305$

Gap between the frame and the inner side of tyre = 152mm

Width of chassis = $1305 - 305$ = 1000mm

The final dimensions of the length and width of the vehile are:

Table 3.7: Chassis frame dimensions

Parameters	Dimension (mm)
Length	4695
width	1000

3.8 Geometry Preparation of the chassis frame

The chassis frame is modelled in Solidworks utilizing the above dimensions. From the calculation, it is obtained that the rectangular hollow section of dimensions 50mm*30mm having a thickness of 5mm could be used for the above-mentioned loading condition. Since the total load is assumed to be divided between the two side beams, each beam is applied with half of the total load to be applied excluding the self-weight of the beam.

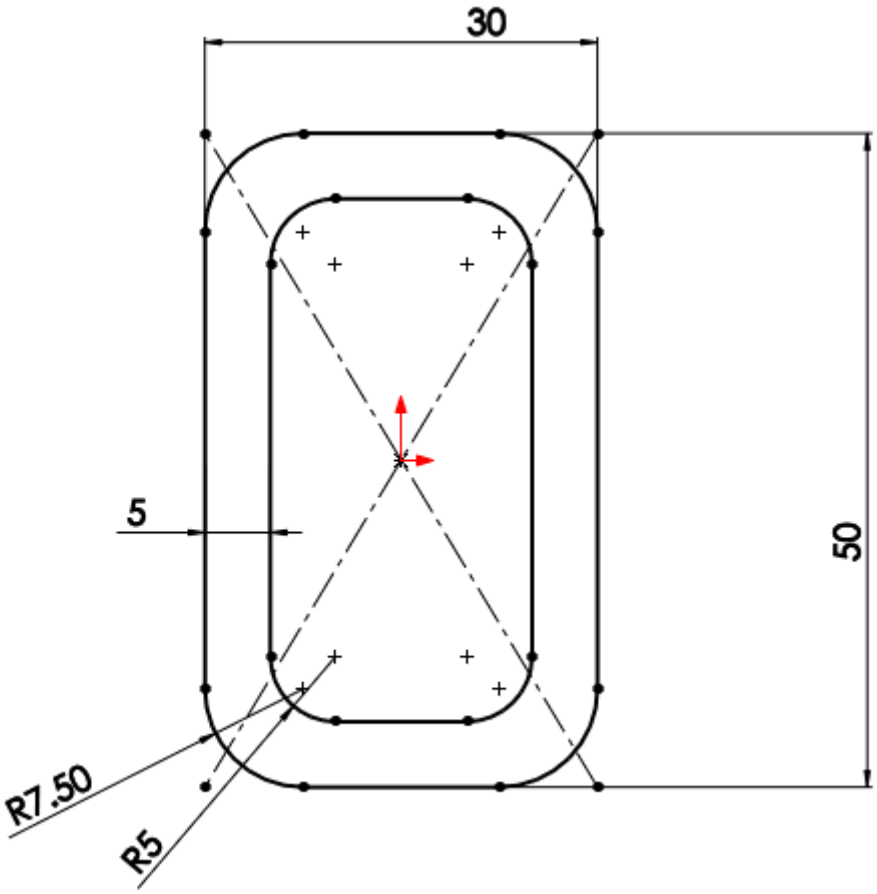

Figure 3.8: Weldment profile of beam

While modelling, only the frame is modelled but not the supporting parts as the supporting parts are to be represented using the boundary condition in the simulation environment. A weldment tool is used to create the frame as the members of the frame will be attached using the welded connection in real life as well. Members of the frame are touched at the surface but due to the presence of fillet on the weldment profile, there was a gap between the side members and the cross members. The cross members are extended to touch the side member using the trim command under the weldment tab. To apply for the fixed support, the rectangular split of 15*60 is created on the bottom face of the side beam. This split will only split the bottom layer of the side beam to make a face where fixed support could be applied while applying boundary conditions.

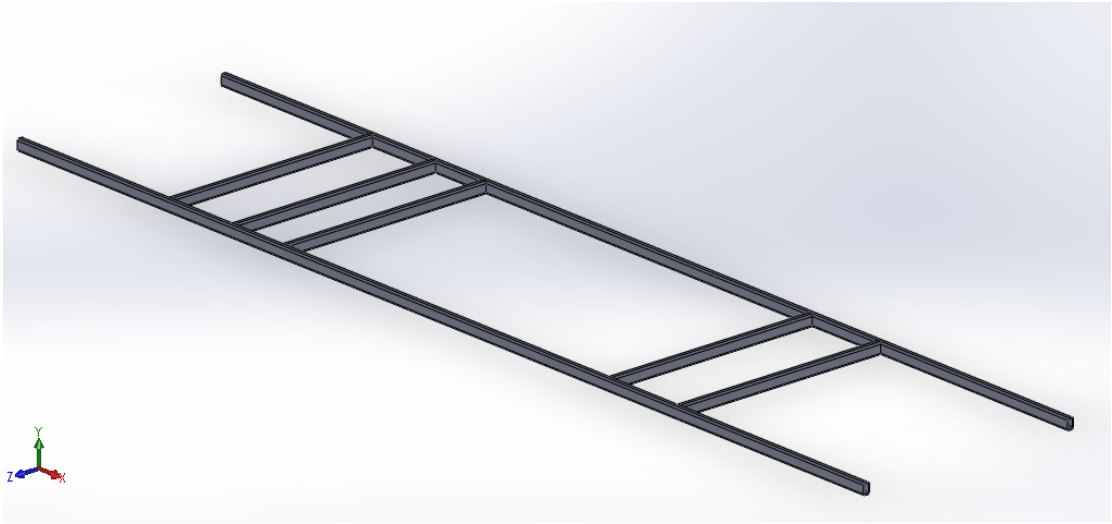

Figure 3.9: Preliminary model of chassis

Chapter 4: MODELLING AND SIMULATION

Ansys is used to perform the finite element analysis on the chassis frame. FEM includes the following steps.

1. Preprocessing
2. Solution
3. Post-processing

4.1 Preprocessing

4.1.1 Geometry

The CAD model of the frame is prepared in SolidWorks and the geometry cleanup is performed using the tools available in it. The model is saved in .step format and imported to the Ansys static structural inside geometry. The model has a total weight of 75.183kg. The same model as shown in the geometry prepration section is used for analysis.

4.1.2 Meshing

Ansys Mechanical is started, and the mesh is generated. For the initial simulation, meshing is set to default coarse meshing and the connection between the parts is checked. Bonded connection is applied between the contact and target faces and the behaviour is set to program controlled which is auto-asymmetric by default. Auto asymmetric allows the program to evaluate the contact region and select the surface to mesh with contact elements and target elements. After running the solver for coarser mesh, refinement is added and then the solver is run again.

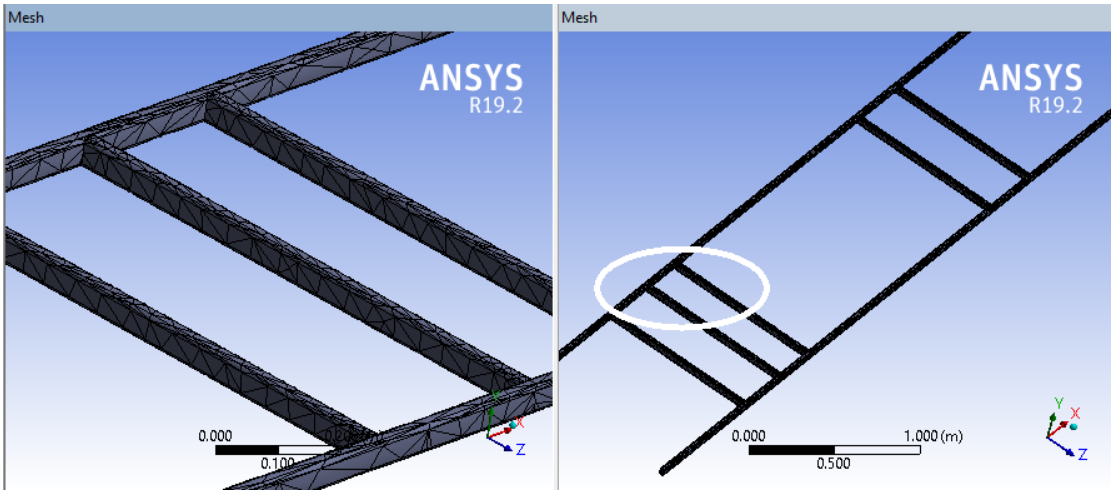

Figure 4.1: Default mesh

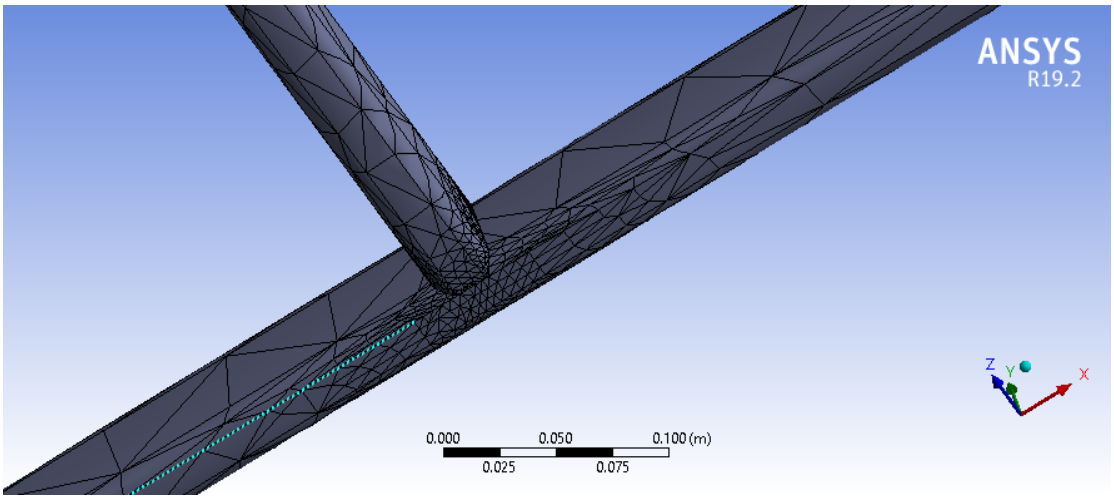

Figure 4.2: Mesh with refinement

Table 4.1: Mesh statistics

Statistics	
Nodes	51151
Elements	27473

4.1.3 Boundary conditions

Applying the right boundary conditions is an essential part of getting good simulation results. Since the connection of the chassis frame with the tyre of the vehicle through the suspension system is not modelled in geometry, it should be represented carefully

using the right type of support. For the support, the split geometry is used, and fixed support is applied at the split face. Such four faces are created where the suspension system touches the chassis frame. This is shown in the figure below.

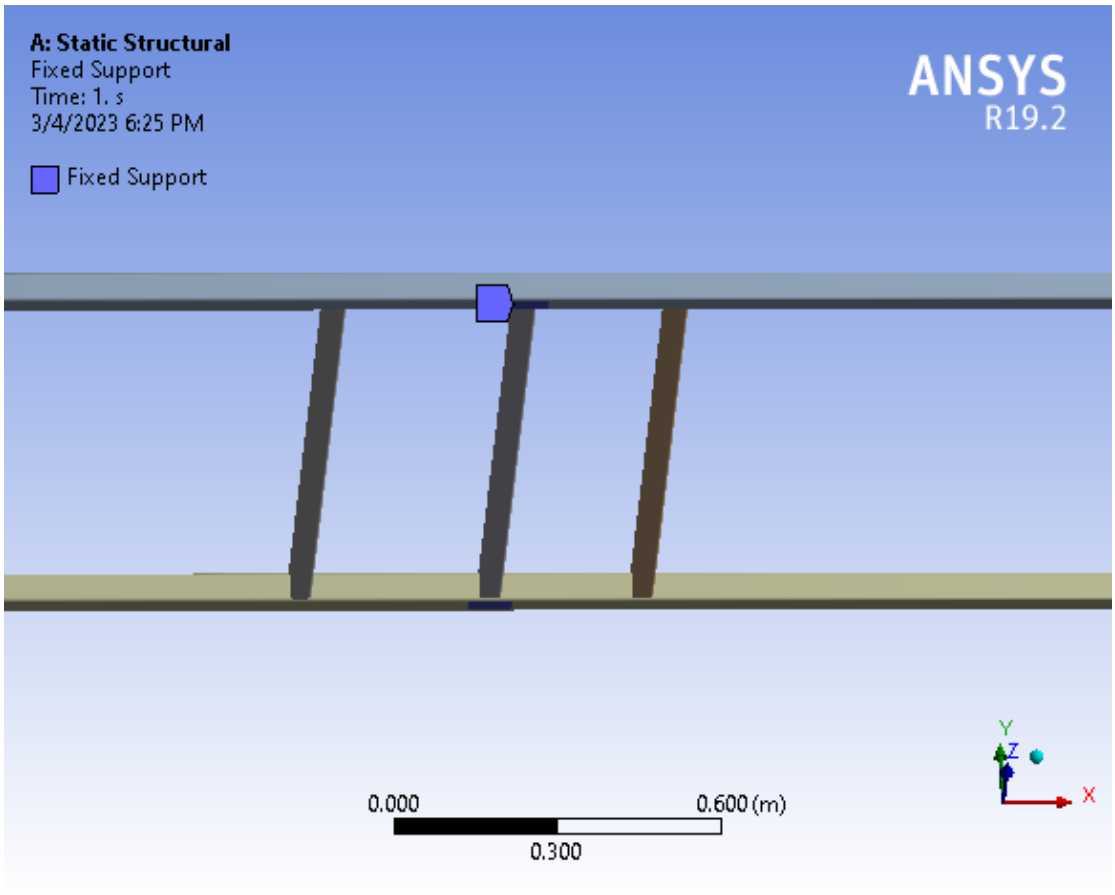

Figure 4.3: Fixed support

Load is applied on the frame as stated earlier in the chassis load intensity section.

Table 4.2: Load applied over frame

Load type	Load Intensity(N)
Battery load on mid-section	5644
Distributed load throughout the frame	1855
Motor concentrated load	800
Controller concentrated load	800
Self-weight due to gravity	751.8
Total load	26550.8

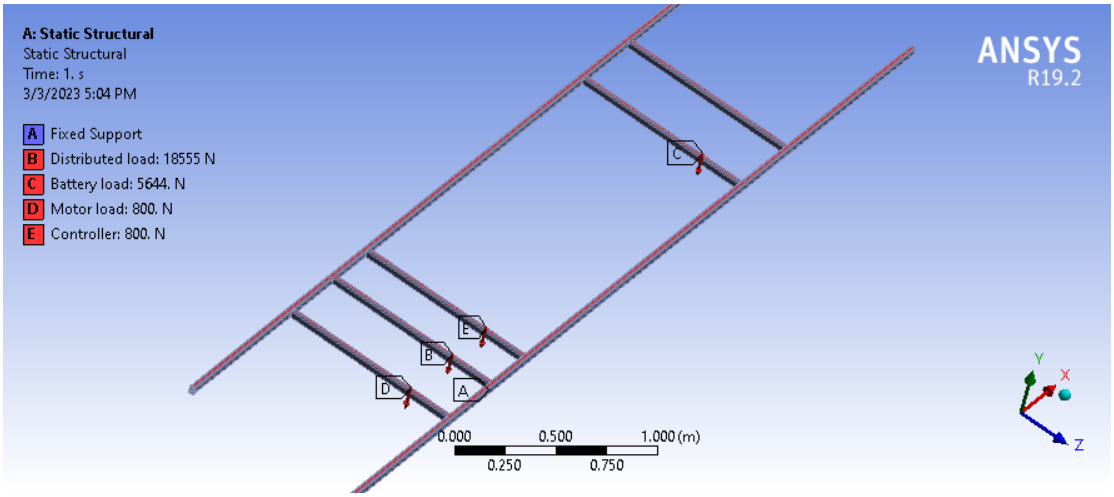

Figure 4.4: Load present on chassis frame

4.2 Solution

This step is done by ANSYS mechanical. It considers all the input provided to it in the form of material assignment, connections between the parts, elements to be used for simulation, the total number of nodes and elements, loading and constraints. Considering all these things, Ansys mechanical perform finite element analysis. The results would be reliable if the given input is correct as it follows the concept of GIGO. Thus the solutions obtained from the simulation must be validated and verified. This is the last step of FEA.

4.3 Post-processing

The solution obtained from the analysis could be viewed using several contour plots or graphs. The equivalent stress plot is generated and the averaged equivalent stress and unaveraged equivalent stress plots are viewed. In this case, the two values are quite different, which shows that the solution obtained is not the mesh-independent solution. Thus, we need to refine the mesh further. Further mesh refinement is done on the region of maximum stress and on the solution the maximum equivalent stress value kept increasing, also the difference between averaged value and the unaveraged value. The stress singularity is obtained in the region shown below.

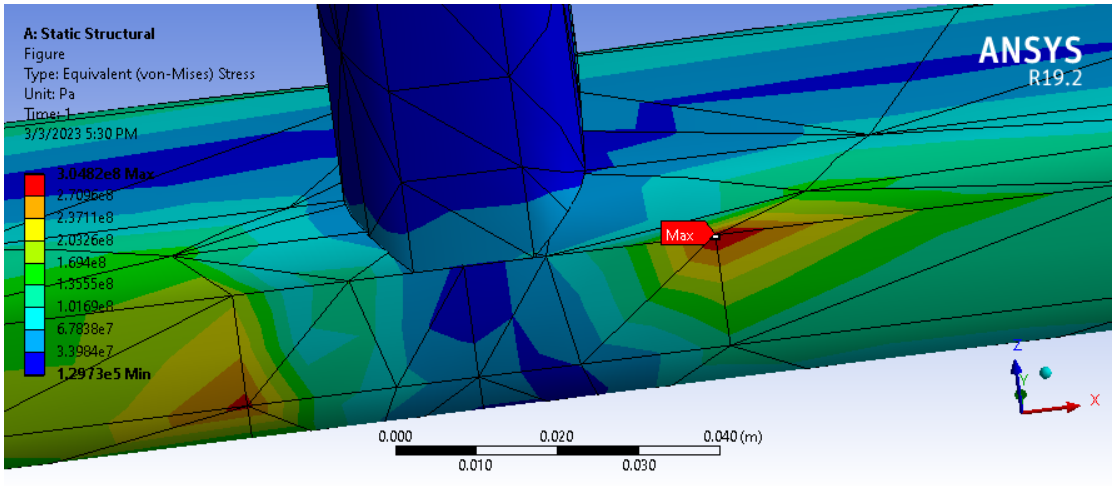

Figure 4.6: Equivalent stress plot showing stress singularity

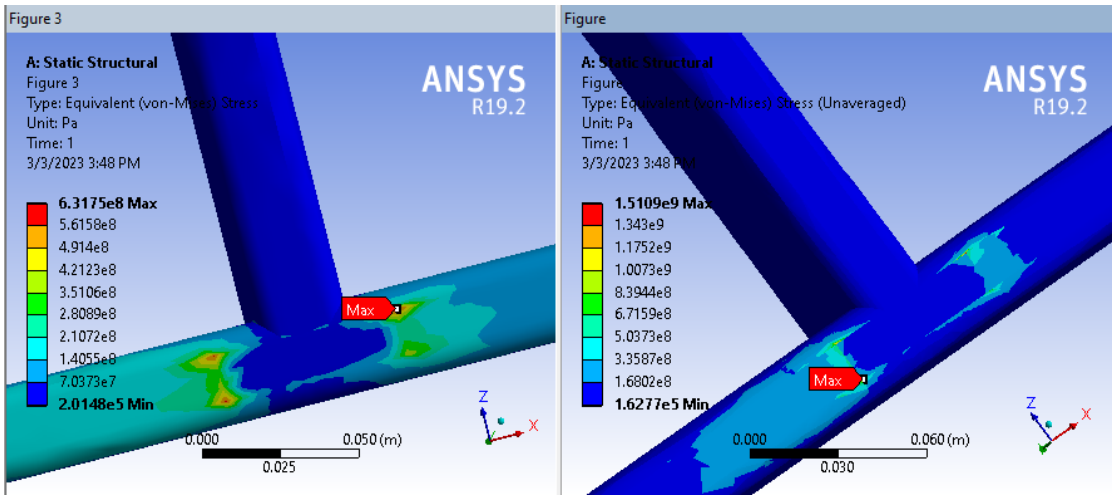

Figure 4.5: Comparison of averaged and unaveraged equivalent stress.

Since the value of maximum equivalent stress did not converge with mesh refinement, thus the solution is not the mesh-independent solution. Without a mesh-independent solution, we cannot validate whether the solution is correct or not. Thus we need to remove the stress singularity from the simulation solution. Stress singularity is observed at the zone of fixed support, thus the way fixed support is applied to the model needs to be changed.

4.4 Analysis of frame with cross-section 50*30 with different fixed support

The split feature applied on the frame is removed as it caused stress singularity. Now, the four ends of the chassis frame are applied fixed support and steps similar to the previous simulation are followed.

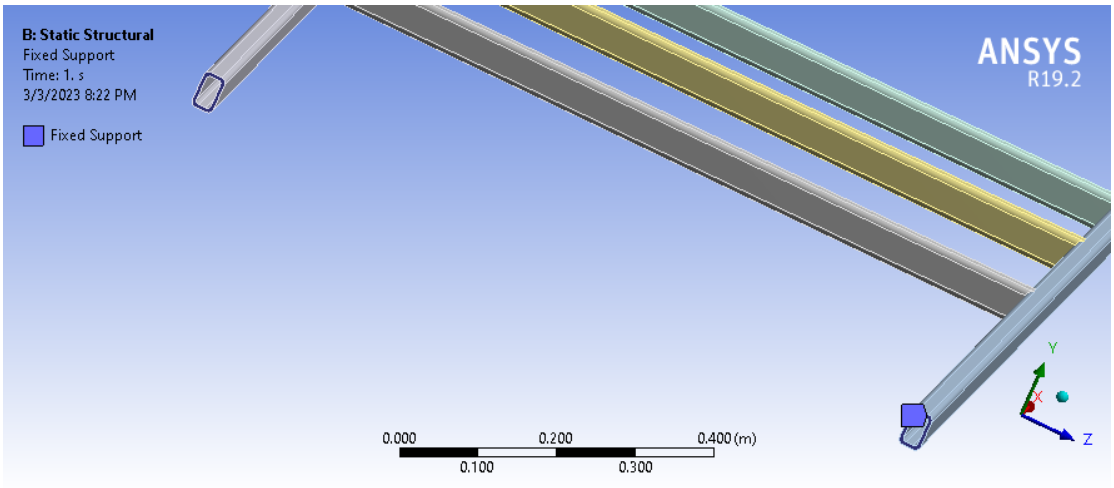

Figure 4.7: Fixed support new position

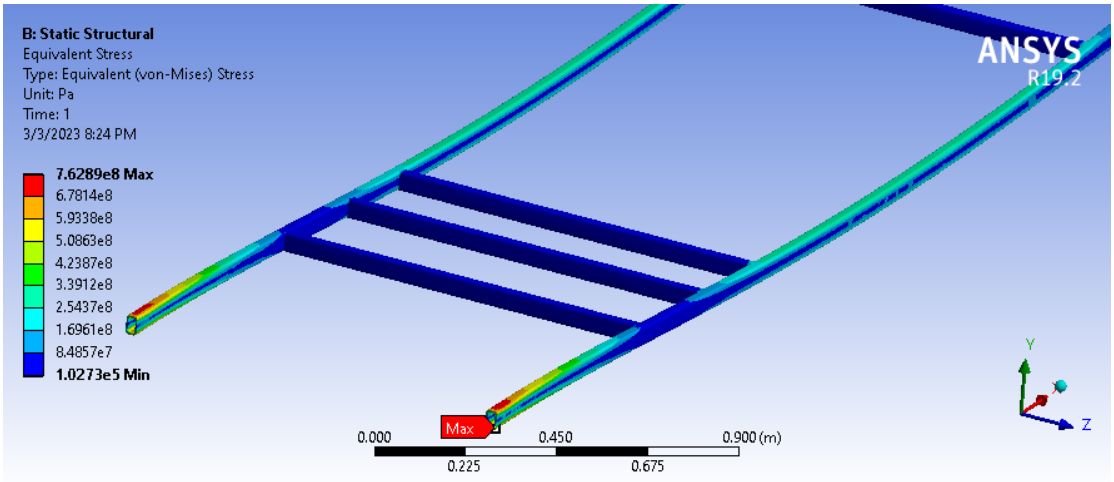

Figure 4.8: Equivalent stress plot averaged

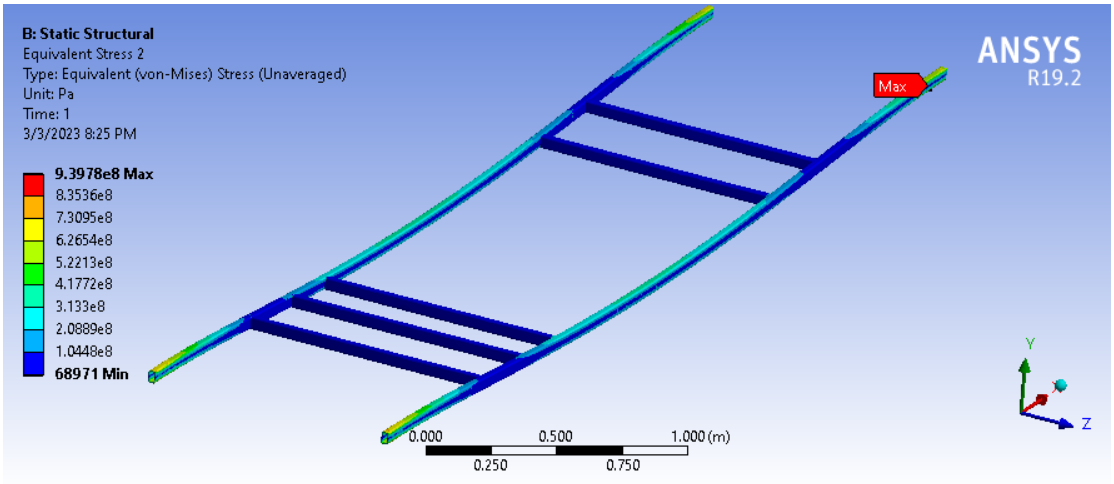

Figure 4.9: Equivalent stress plot unaveraged

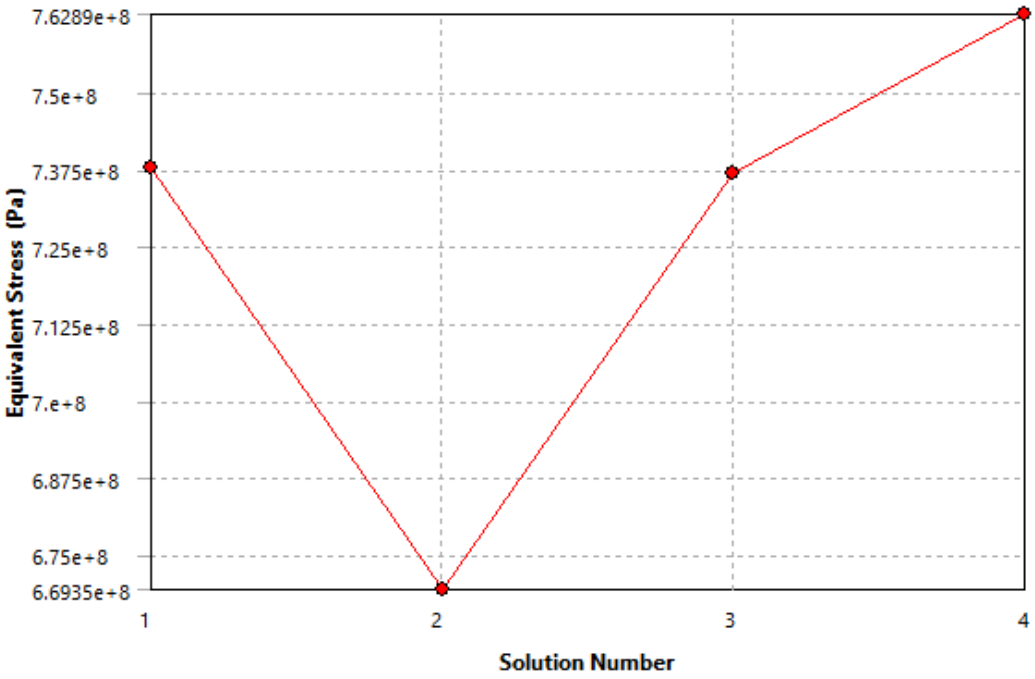

Figure 4.10: convergence plot

Table 4.3: Convergence results

	Equivalent Stress (Pa)	Change (%)	Nodes	Elements
1	7.3792e+008		22460	9516
2	6.6935e+008	-9.7448	104839	59785
3	7.37e+008	9.6207	350669	217355
4	7.6289e+008	3.4523	1099327	725400

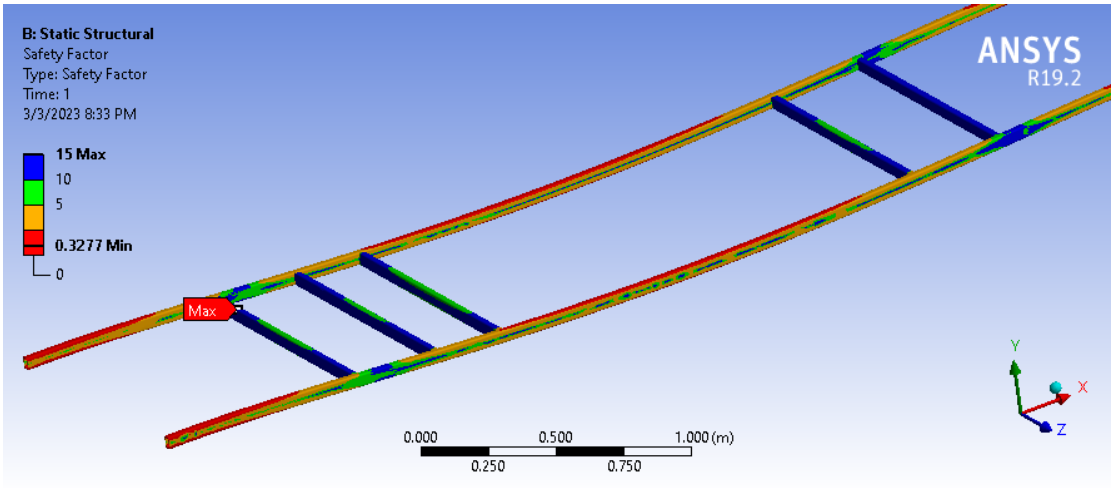

Figure 4.11: Factor of safety

The convergence plot and convergence table show that the convergence occurred and the maximum equivalent stress is obtained to be 762.89 MPa which is more than three times larger than the allowable stress for the structural steel. Due to this, the factor of safety is obtained to be 0.327. Also from the equivalent stress plot it can be seen that maximum stress occurs on the side members of the beam, so we need to select the beam with a sectional modulus value larger than $7.486 * 10^3$ mm^3.

4.5 Design iteration-1

Since the previously selected member yield, we now need to select the frame with a higher sectional modulus than the old one. Let's build the new frame with the rectangular hollow section beam whose sectional modulus value is $10.94 * 10^3$ mm^3.

The chassis frame is designed with the member of higher sectional value and simulation

is performed. The results obtained from the simulation are displayed here.

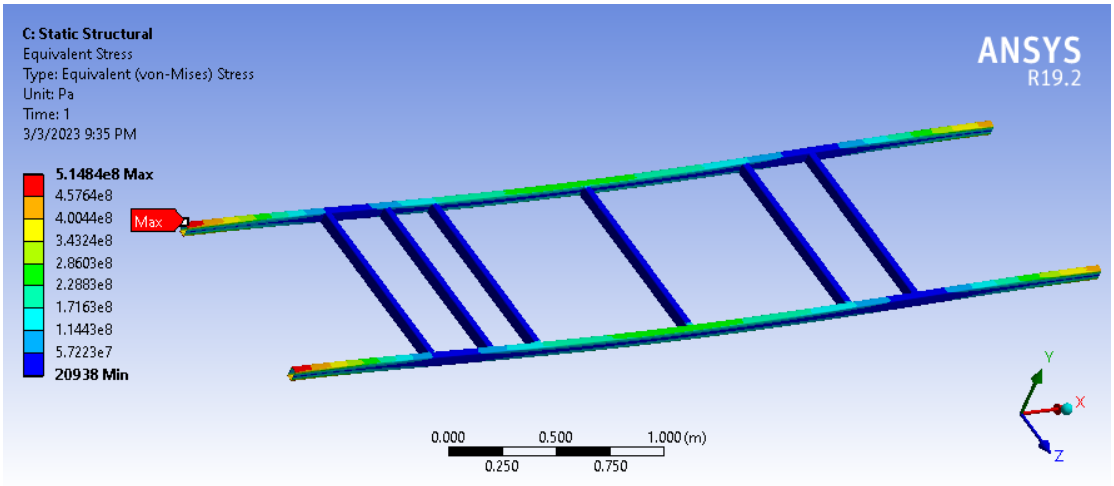

Figure 4.12: Averaged equivalent von-mises stress iteration 1

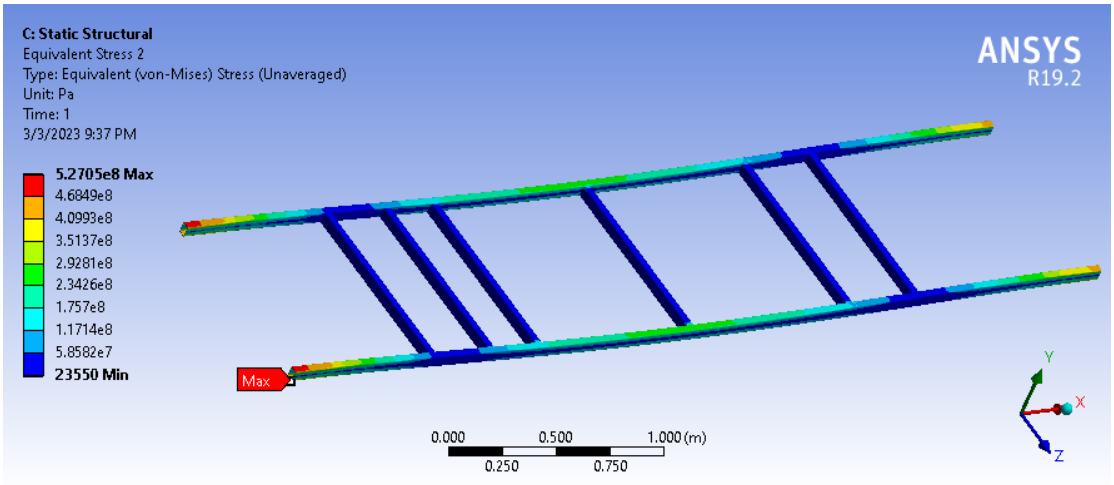

Figure 4.13: Unaveraged equivalent von-mises stress iteration 1

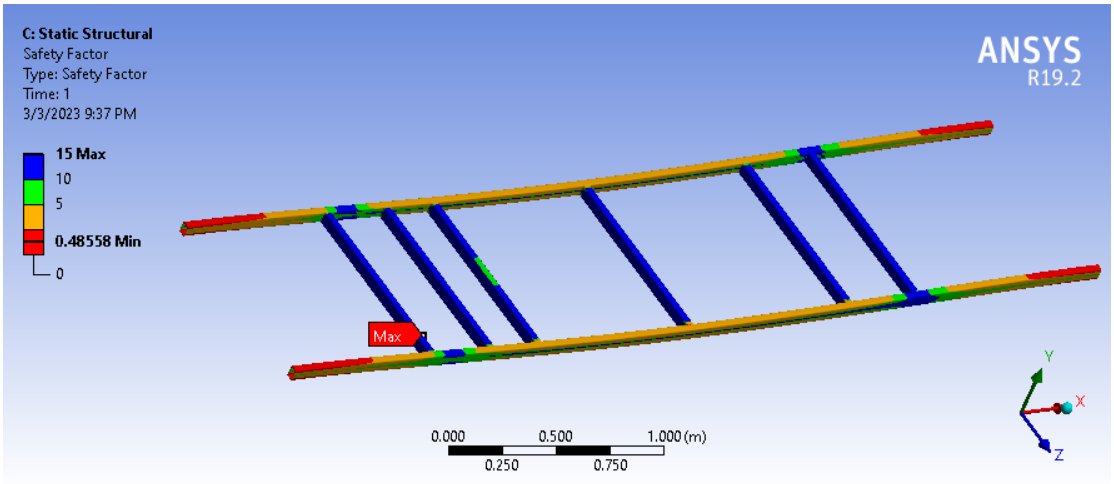

Figure 4.14: Factor of safety iteration 1

In this simulation, the mesh is not refined as the value of maximum equivalent stress is obtained to be larger than the allowable stress, so we can conclude that the frame would yield. This information is enough to reject this frame as well.

4.6 Design iteration 2

The rectangular hollow section with section modulus $10.94 * 10^3$ mm^3 is also rejected as it undergoes yielding under applied loading. From the above two simulations, we know the value of maximum equivalent stress for the given value of the sectional modulus of the beam.

Table 4.4: Determination of required sectional modulus

Sectional modulus($*10^3$ mm^3)	Equivalent Stress(MPa)
7.486	762.89
10.94	514.84
x	200

Using interpolation, we get

$$\frac{y_2 - y_1}{x_2 - x_1} = \frac{y - y_1}{x - x_1}$$

or, $\frac{514.84 - 762.89}{10.94 - 7.486} = \frac{200 - 762.89}{x - 7.486}$

or, $\frac{-248.05}{3.454} = \frac{-562.89}{x-7.486}$

or, $x - 7.486 = 7.8380$

$\therefore x = 15.324$

From the above calculation, It is obtained that the rectangular hollow section with the sectional modulus $15.324 * 10^3 \text{mm}^3$ is suitable and gives the maximum equivalent stress to be 200 MPa.

The available rectangular hollow section is RHS 80*40/4 with a sectional modulus of $17.05 * 10^3 \text{mm}^3$. The simulation results are presented here.

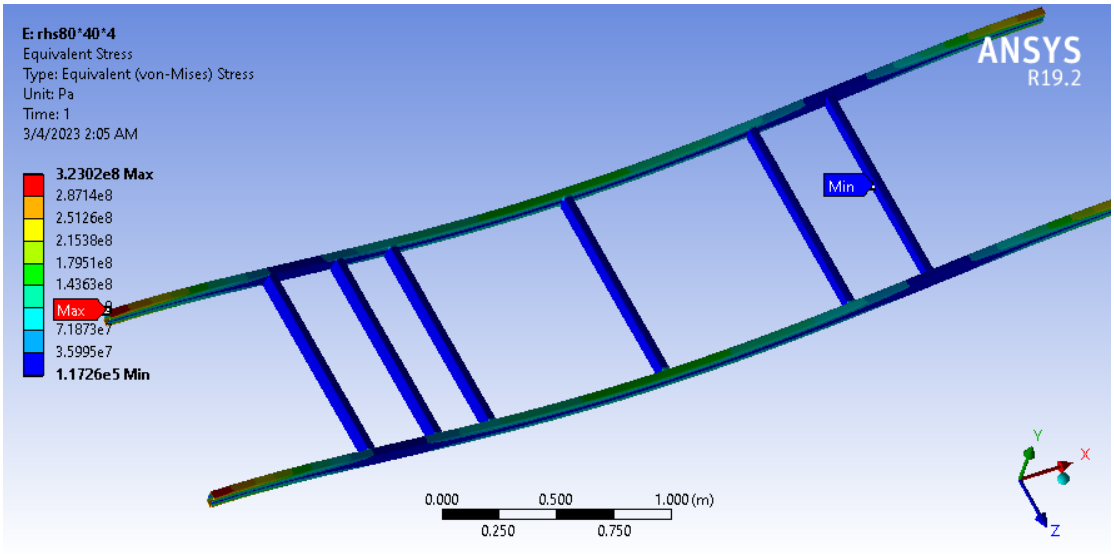

Figure 4.15: Equivalent stress plot

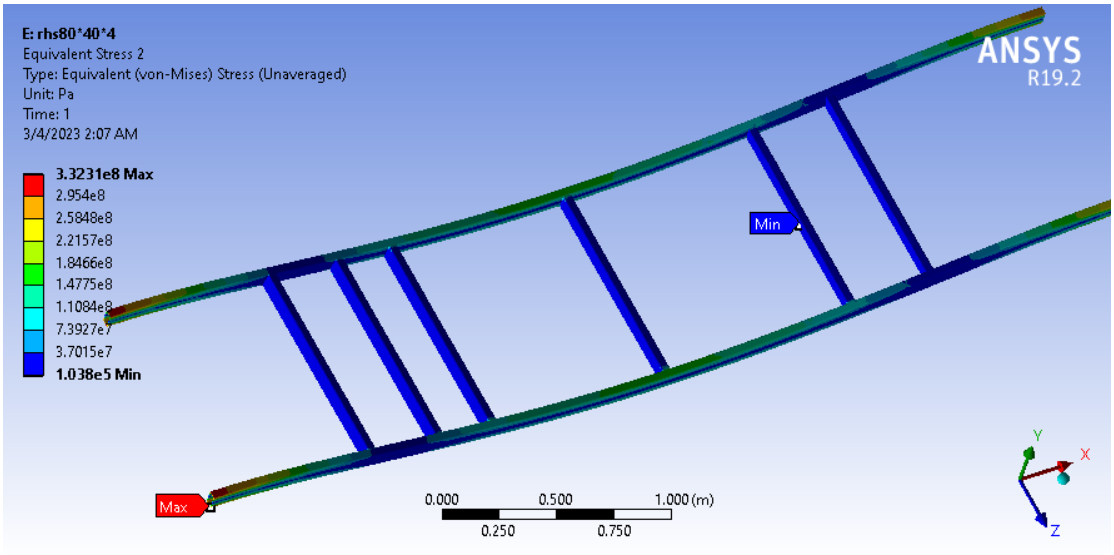

Figure 4.16: Unaveraged equivalent stress plot

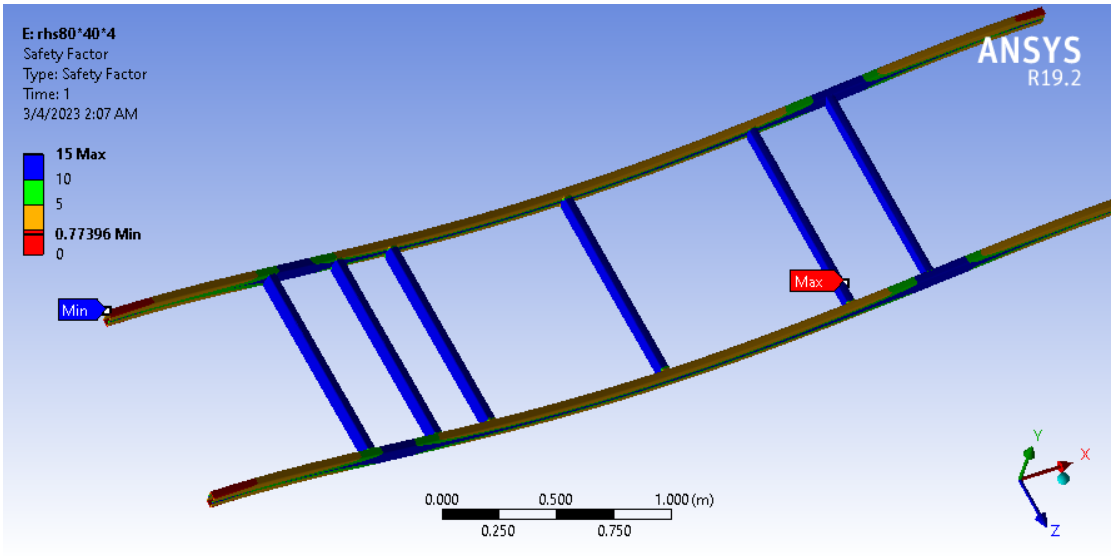

Figure 4.17: Factor of safety plot

The value of maximum equivalent stress came to be 332.14 N/mm^2 which doesn't come under the acceptable range.

4.7 Final Design

Similar iterations are performed to figure out the most suitable one. The main of these iterations is to find out the beam section with a factor of safety around 2.5 for maximum equivalent stress, as it would provide us with a safety margin of 1.5. After the number of

simulations, we finally selected the beam with the sectional modulus of 87.54 $*10^3 mm^3$.

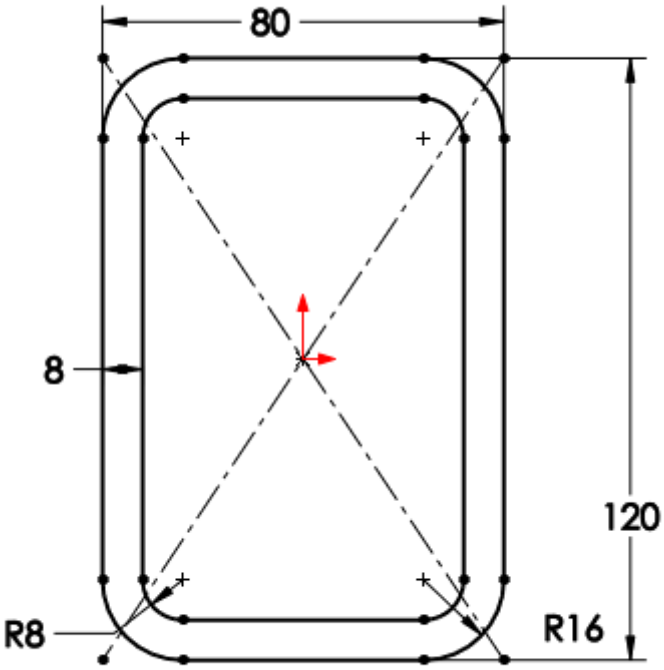

Figure 4.18: Weldment profile RHS 120*80*8

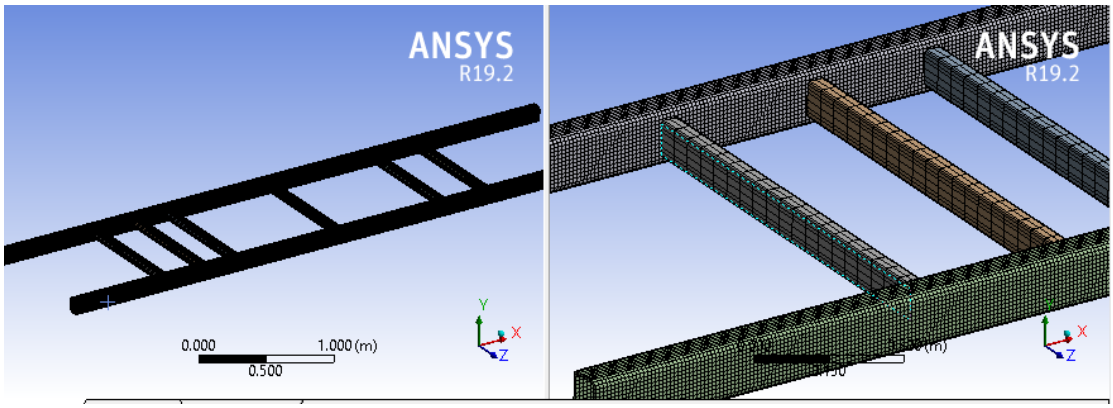

Figure 4.19: Meshing in final design

Mesh Metric	Jacobian Ratio (Corner Nodes)
Min	0.23823
Max	1.
Average	0.85191
Standard Deviation	0.22822

Figure 4.20: Mesh metric: Jacobian ratio

Mesh Metric	Orthogonal Quality
Min	0.5615
Max	1.
Average	0.98239
Standard Deviation	6.2589e-002

Figure 4.21: Mesh metic: Orthogonality ratio

Mesh Metric	Skewness
Min	1.3057e-010
Max	0.82045
Average	7.4041e-002
Standard Deviation	0.1181

Figure 4.22: Mesh metic: Skewness

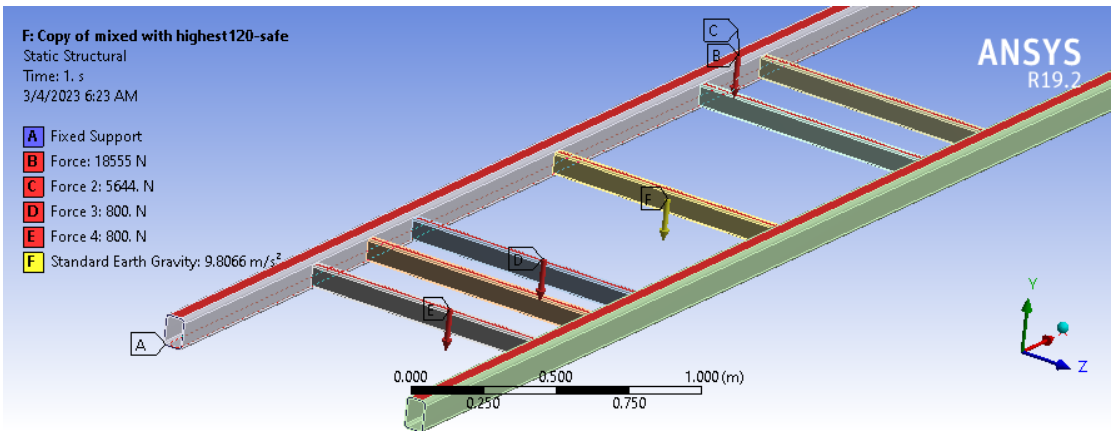

Figure 4.23: Load application on final model

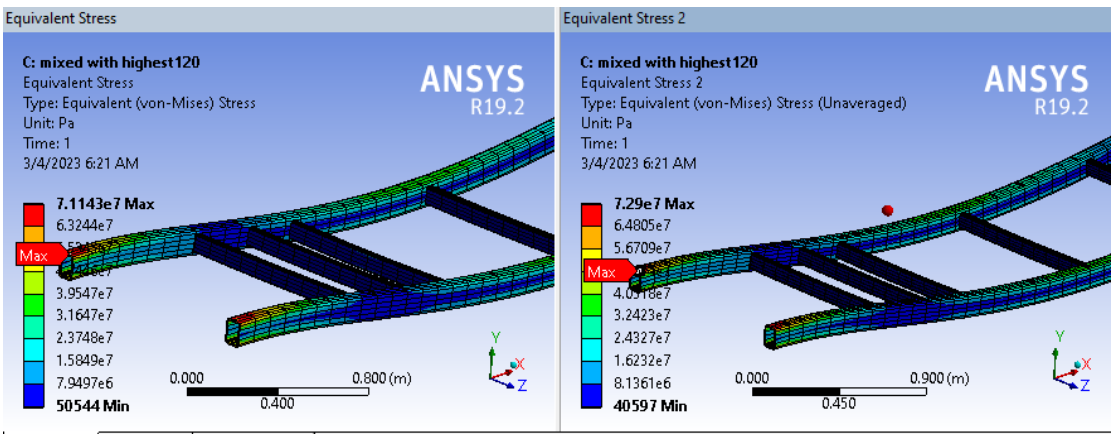

Figure 4.24: Equivalent stress averaged and unaveraged without mesh refinement

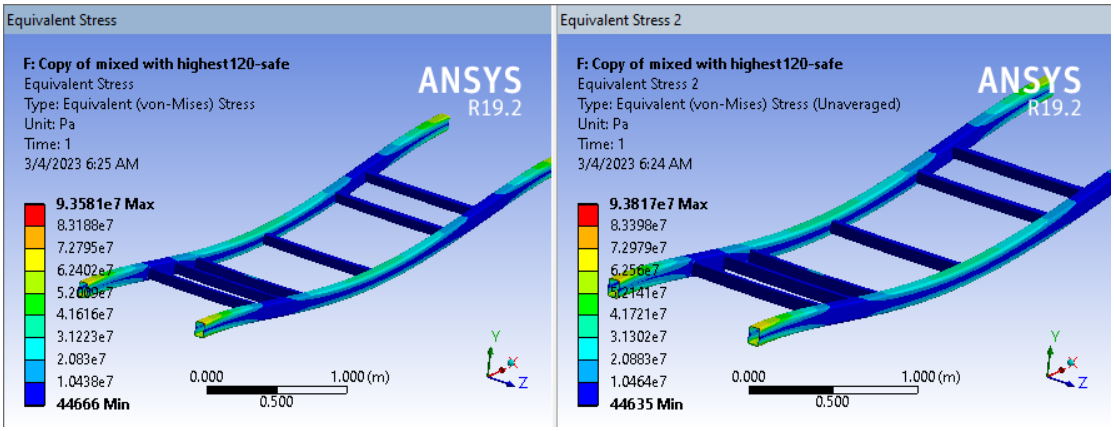

Figure 4.25: Averaged and Unaveraged equivalent von-mises stress with mesh refinement

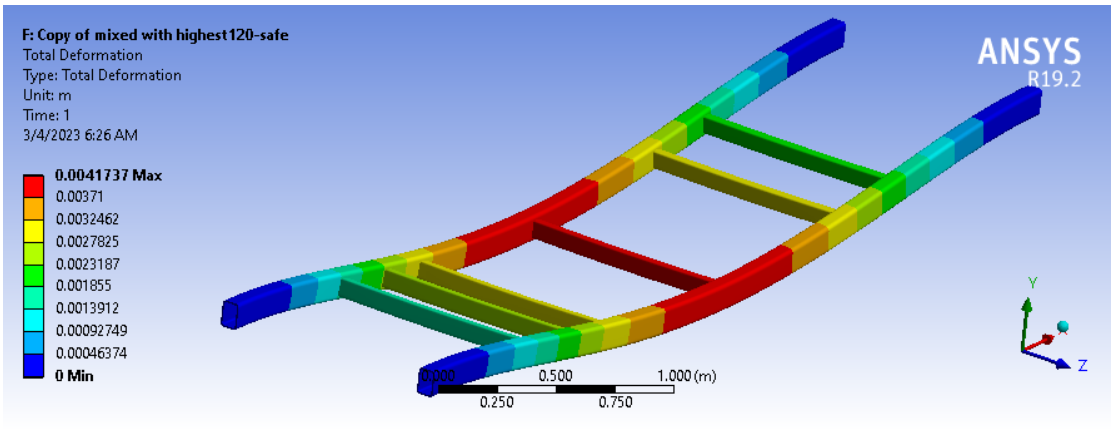

Figure 4.26: Deformation in frame

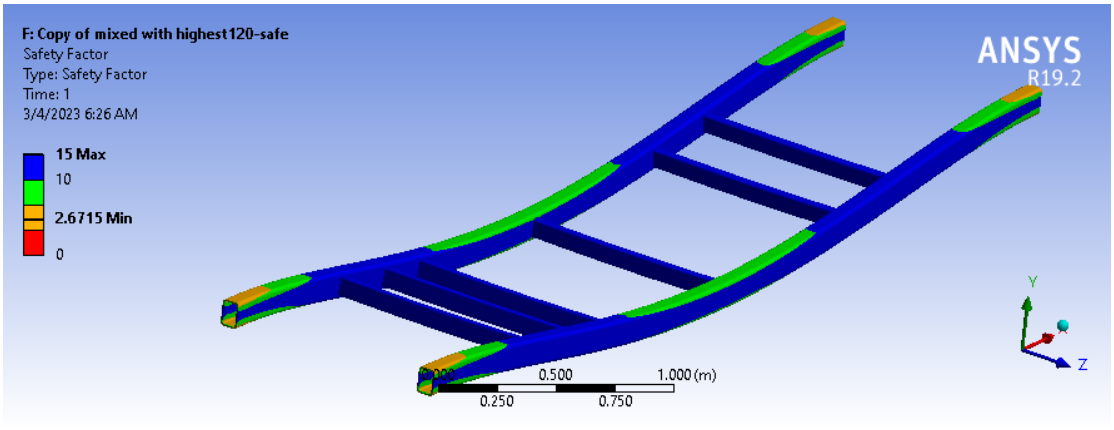

Figure 4.27: Maximum equivalent stress factor of safety

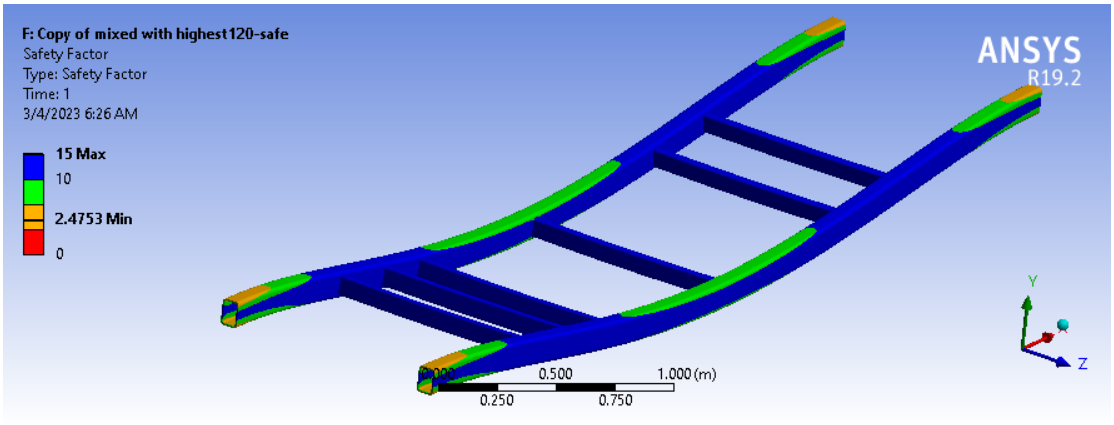

Figure 4.28: Maximum shear stress factor of safety

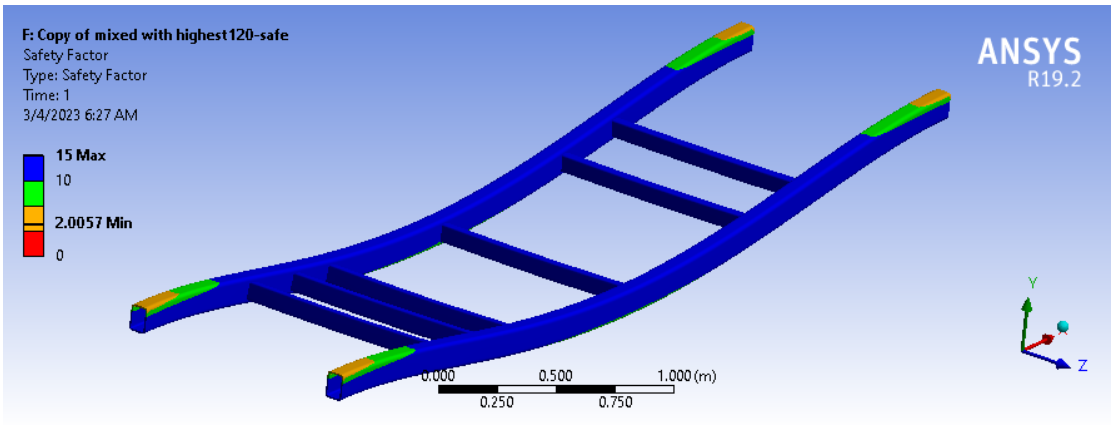

Figure 4.29: Maximum tensile stress factor of safety

The maximum equivalent stress is obtained to be 93.58 N/m^2, maximum deformation of 4.1737 mm. The factor of safety is 2.6715 for maximum equivalent stress, 2.4753 for maximum shear stress and 2.0057 for maximum tensile stress.

Chapter 5: RESULT AND DISCUSSION

5.1 Summary of all design iterations

This table summarizes the data obtained from all the design iterations.

Table 5.1: Summary of design iterations

S.N.	Profile	Elastic Section modulus($*10^3$ mm^3)	Maximum Equivalent Stress (MPa)	Mass (kg)	Factor of Safety
0	RHS 50x30 /5	7.486	762.89	75.183	0.3277
1	RHS 60x40 /4	10.94	514.48	85.465	0.4855
2	RHS 80x40 /4	17.05	323.02	104.49	0.77396
3	RHS 100x60 /5	37.82	237.55	174.17	1.0524
4	RHS 120x80 /8	87.54	93.58	242.4	2.6715

The final design of the chassis frame is used and the components of electric vehicles are assembled using SOLIDWORKS to provide the visual display of the location of several components.

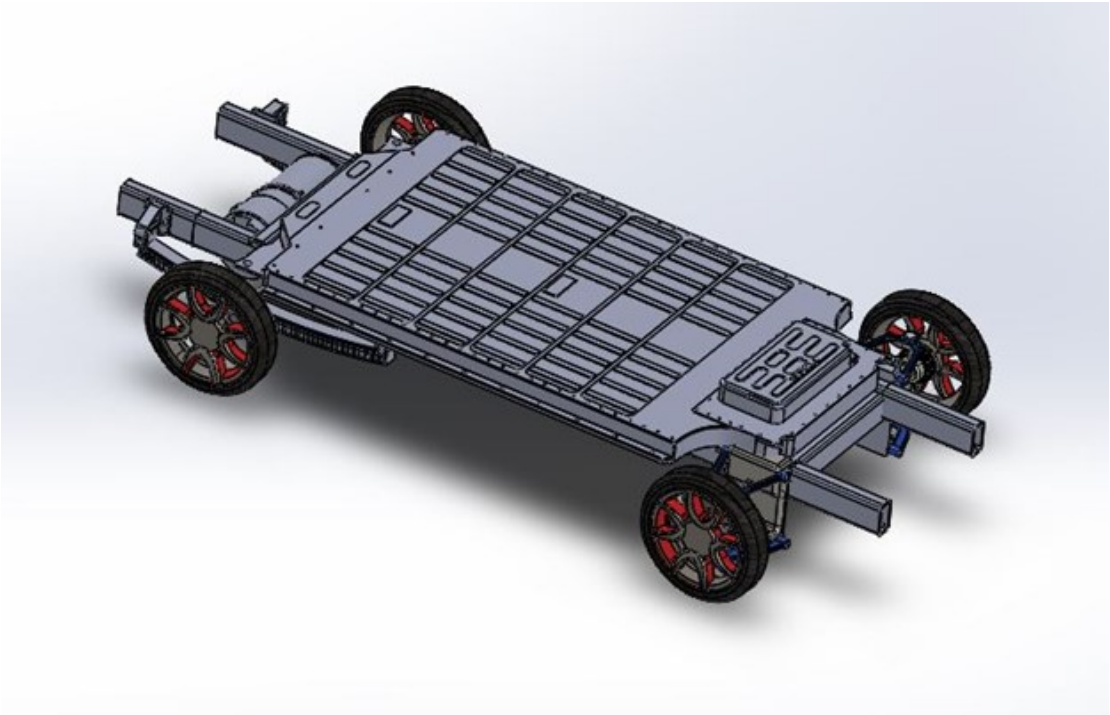

Figure 5.1: Final design of the chassis frame

5.2 Validation of Simulation results

The results obtained from the simulation need to be validated before those results could be trusted and used in inferring anything. The numerical accuracy is ensured by generating a mesh-independent solution. In the first simulation, we inserted a convergence tool to converge the results with a 5% relative error. This ensured the mesh-independent solution. But this process turned out to be computationally expensive, so instead of using an iterative solver, we tried refining mesh manually with the use of different meshing features such as face meshing and sizing and obtained refined mesh. Then to check, whether the refinement is enough or not we compared the averaged and unaverage maximum equivalent stress values. When these values were near to each other, we obtained a mesh-independent solution. In this way, The simulation results are validated.

The allowable value of deformation for a beam under bending is given by $\frac{l}{300}$ [38]. In this case, the value of l is 4695mm. Hence, the allowable deformation is 15.65mm. From the simulation, the deformation is obtained to be 4.17mm. Thus, the deformation is within the elastic limit.

5.3 Modal Analysis

Modal analysis is performed to study the behaviour of the frame in response to vibration and dynamic loading. To study the dynamic behaviour, the natural frequencies and mode shapes of the frame are determined. Modal analysis is of two types: free-free or constrained. In a free-free analysis, the natural frequencies and mode shapes are calculated without applying any boundary condition. In a constrained analysis, the analysis is done by applying boundary conditions to imitate the actual working condition of the vehicle. We use ANSYS to perform the modal analysis.

The following table shows the first ten-order natural frequencies

Table 5.2: Natural frequency of the frame

S.N.	Natural Frequency	Maximum Deformation	Description
1	26.444Hz	3.1518mm	The frame is subjected to vertical bending
2	31.097Hz	3.2373mm	The frame is subjected to vertical bending
3	43.03Hz	3.5422mm	The frame is subjected to torsion
4	62.499Hz	2.963mm	The front of the frame is bent vertically
5	81.272Hz	3.1985mm	The rear of the frame is bent vertically
6	99.439Hz	3.2584mm	The frame is subjected to bending and torsion
7	119.13Hz	3.073mm	The frame is subjected to bending and torsion
8	154.4Hz	3.9362mm	The frame is bent vertically
9	179.15Hz	3.2067mm	The frame is subjected to bending and torsion
10	208.21Hz	3.0482mm	The frame is subjected to lateral bending

Frame modal analysis result:

The frequency of some excitation forces that may resonate with the frame are given below:[39]

Excitation frequency of roads -3Hz.

Reducer and transmission excitation frequency - 8.5Hz.

Wheel unbalance excitation- 9Hz

Drive shaft vibration- 46Hz

Table 9.1 shows the natural frequency in the range of 26.44 to 208.44Hz. The frame avoids the above-mentioned excitation frequencies. So, the resonance is avoided which may cause undesirable distortion of the frame.

The first two mode shapes are shown in figure:

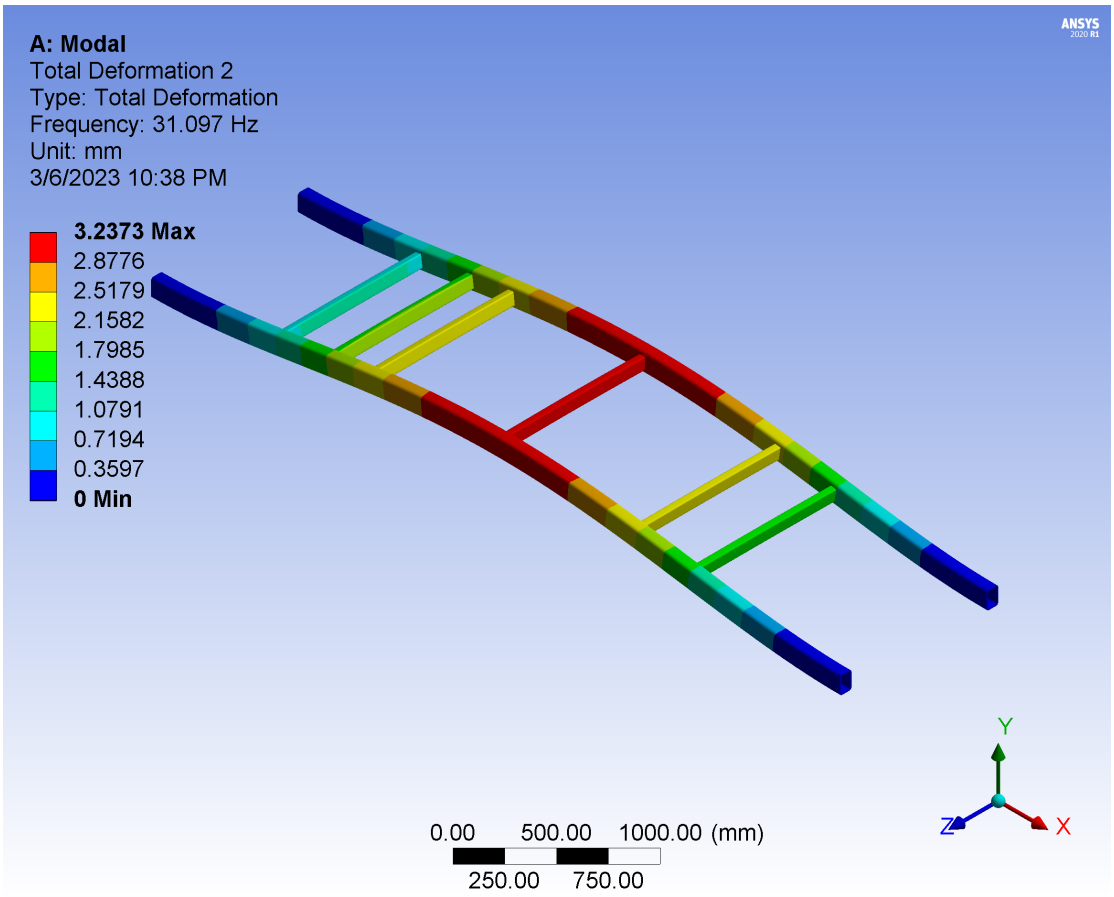

Figure 5.2: 1st modal frequency

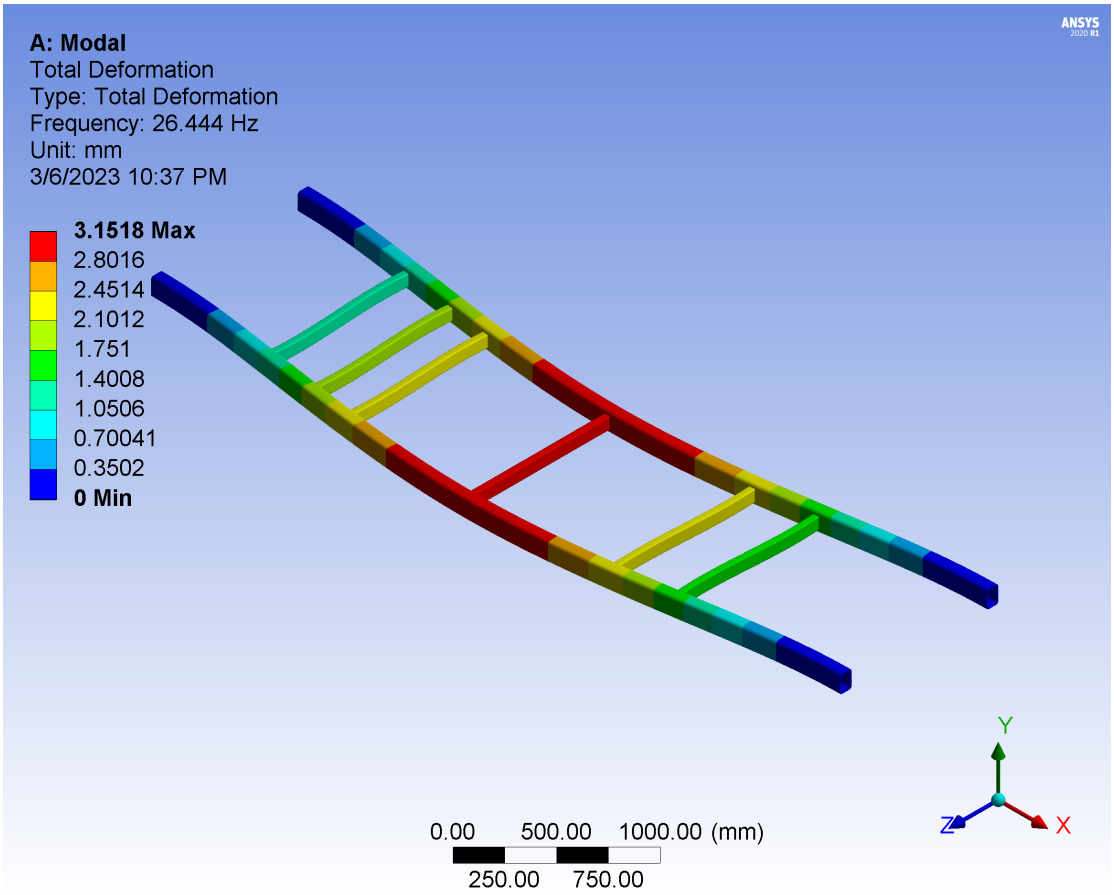

Figure 5.3: 2nd modal frequency

The beam with the sectional modulus of 17.05 is selected to model the cross-members and the one with a sectional modulus of 87.54 is selected for the two side members.

5.4 Bending stiffness

Bending stiffness is the property of the vehicle and it is independent of the load applied to it. So, the bending stiffness of the chassis frame is calculated by an applied load of 1000N at the centre of the frame with a fixed support on the four ends. The deformation value is noted and the following formula is used to find out the bending stiffness.

Bending stiffness, (EI) = $\frac{a^3 * F}{48 * \delta}$, where

a = distance between front and rear restraining points = 4695mm,

F= Force applied on the frame

δ = Deformation obtained.

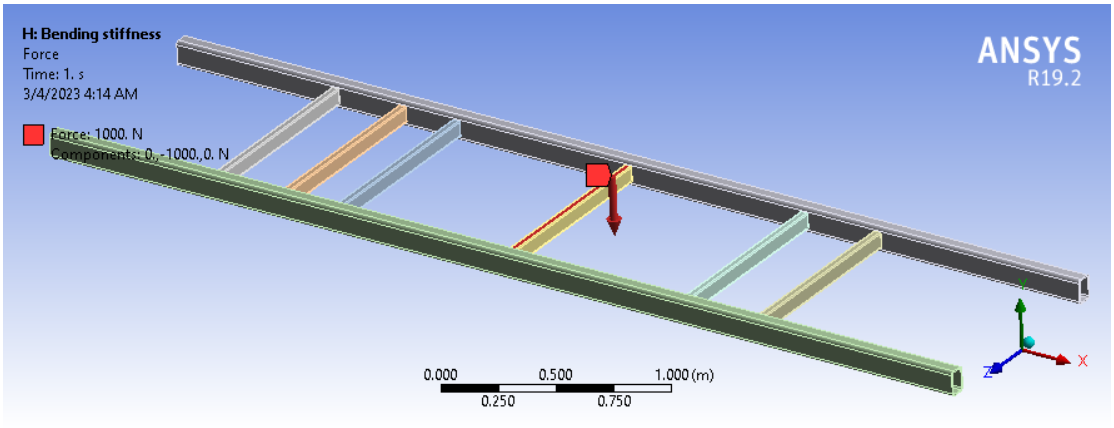

Figure 5.4: Force application to calculate bending stiffness

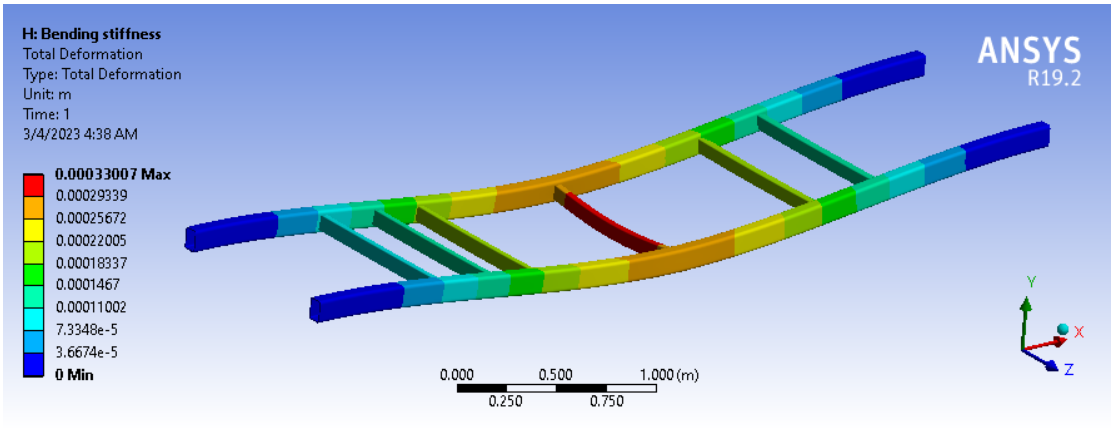

Figure 5.5: Bending stiffness deformation simulation

Simulation results showed that the deformation obtained to be 0.33mm Hence substituting the values in the bending stiffness equation, we get Bending stiffness to be $6.5197 * 10^6 \text{Nm}^2$.

5.5 Torsional Stiffness

Torsional stiffness is also independent of the load applied to the chassis frame. To determine the torsional stiffness of the vehicle, we apply a load of 1000N on both sides of the frame with a fixed support at the rear for front torsional stiffness and the opposite for rear torsional stiffness. The formula used to determine the torsional stiffness is:[15]

Torsional Stiffness, (K_T)=$\frac{T}{\theta}$, where

$\theta = arctan\frac{\delta}{L}$

L= distance between two lateral points of load application.

T=F*d =1000*1 = 1000 Nm

5.5.1 Front Torsional Stiffness

Front torsional stiffness is obtained by applying for fixed support on the rear ends and applying a couple on the front part. The deformation is noted and using the value of applied load and deformation in the torsional stiffness calculation formula, torsional stiffness is determined.

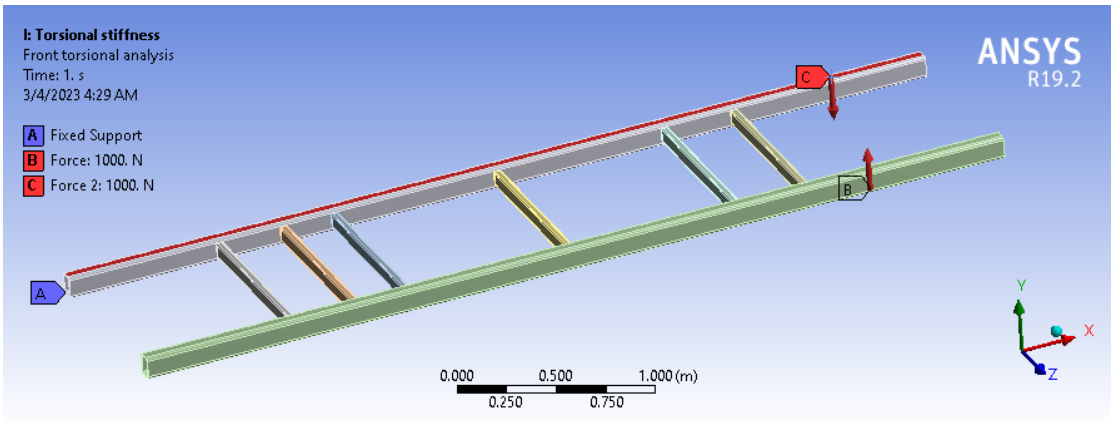

Figure 5.6: Load application to determine front torsional stiffness

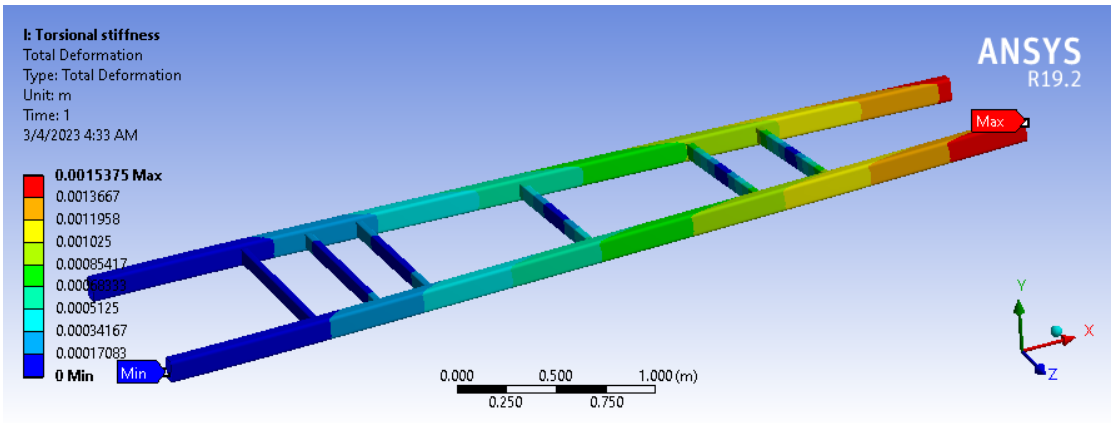

Figure 5.7: Deformation for front torsional stiffness

From the simulation results, δ is obtained to be 1.5375 mm for front torsional stiffness. Applying the value in the torsional stiffness formula, we get the value of front torsional

stiffness to be $6.50407 * 10^5$ Nm/rad.

5.5.2 Rear Torsional Stiffness

Rear torsional stiffness is obtained by applying a couple on the rear side of the frame while keeping the front ends of the frame fixed. A similar formula is used to calculate rear torsional stiffness as per the front torsional stiffness.

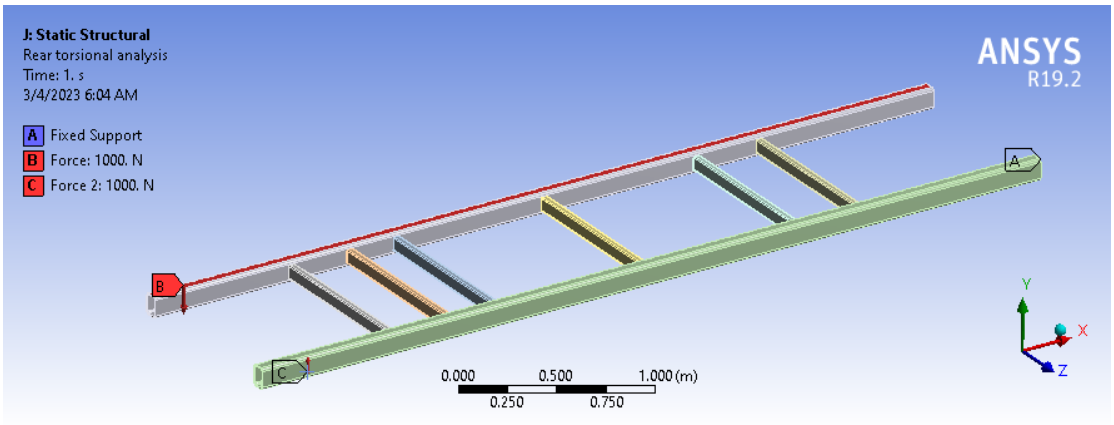

Figure 5.8: Load applicaiton to determine rear torsional stiffness

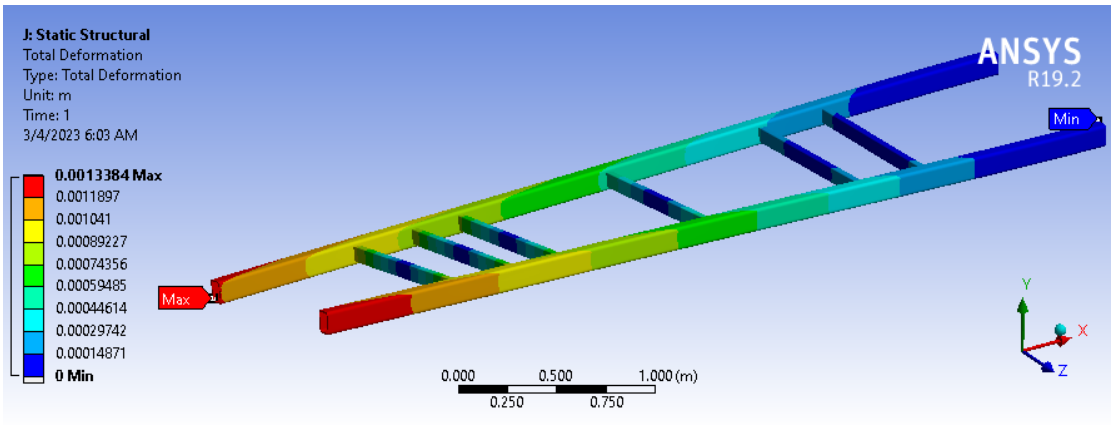

Figure 5.9: Deformation to determine rear torsional stiffness

The value of deformation is obtained to be 1.338 mm for the rear torsional stiffness test. Applying the value in the torsional stiffness formula, we get rear torsional stiffness to be $7.47384 * 10^5$ Nm/rad.

From the literature review, the safe values for bending stiffness, front torsional stiffness and rear torsional stiffness need to be in the range of $4.62 * 10^6$ Nm^2, $5.44 * 10^4$ Nm/rad

and $5.49 * 10^4$ Nm/rad [15]. The values obtained for the chassis frame designed here are larger than the value obtained from the literature review, so we can conclude that the frame is safe to use.

Chapter 6: CONCLUSION AND RECOMMENDATION

6.1 Conclusion

From the material selection portion using the Ashby chart, the carbon steel family is selected as the suitable material for the fabrication of chassis frame. Among the members of the carbon steel family, ASTM A 36 Structural Steel is chosen. The final model is selected after performing finite element analysis on the chassis frames of different cross-sections with varying sectional modulus values. The total load of 28223N including the self weight of the chassis frame is applied to the final model. A rectangular hollow section beam of sectional modulus 87.54 mm^3 with dimensions 120*80/8 is selected for side members whereas the rectangular hollow beam of sectional modulus 17.05 mm^3 with the dimension of 80*40/4 is selected for cross-links. The mass of the final model is obtained to be 242.4 kg.

The bending stiffness of the chassis frame is obtained to be $6.5197*10^6$ Nm^2 and the front and rear torsional stiffness of the chassis frame are obtained to be $6.50407*10^5$ Nm/rad and $7.47384*10^5$ Nm/rad respectively. Hence, the chassis frame is safe for vertical bending with Maximum equivalent stress of 93.58 N/m^2, maximum deformation of 4.1737mm The factor of safety is 2.6715 for maximum equivalent stress, 2.4753 for maximum shear stress and 2.0057 for maximum tensile stress. Thus, we can say that the chassis is safely designed for these three failure criteria.
Also, From Modal Analysis, It is observed that the natural frequency of the frame came to be far from the external excitation frequency. Hence, the frame won't break down due to resonance.

6.2 Recommendation

We have limited our study to the design and static analysis of the electric vehicle chassis frame. In future, the following works could be done to further improve the design and performance of the electric vehicle chassis.

1. The effect of the suspension system is ignored while performing the static analysis of the vehicle, so one could incorporate the effective suspension system.

2. The frame is only analyzed for static conditions, so analysis could be done to ensure vehicle safety in moving conditions as well.

3. Analysis for failure is not done in this study, so possible modes of failure analysis could be done and current design could be modified on that basis.

Bibliography

[1] M. Kimberley, "Here's why a ladder chassis is so right for off-roaders," Nov 2018.

[2] "Body: Lighter and stiffer."

[3] "Unit 1 types of automobiles notes automobile engineering - aryabhatta knowledge university bihar-mechanical engineering-engineering sem-1 (2022): Goseeko."

[4] K. Rangam, "Types of car chassis explained: From ladder to monocoque!," Dec 2022.

[5] C. Hammerschmidt, "Hyundai challenges vw with bev platform," Dec 2020.

[6] H. Hazimi, Ubaidillah, A. E. P. Setiyawan, H. C. Ramdhani, M. Z. Saputra, and F. Imaduddin, "Vertical bending strength and torsional rigidity analysis of formula student car chassis," in *AIP Conference Proceedings*, vol. 1931, p. 030050, AIP Publishing LLC, 2018.

[7] G. Saldaña, J. I. San Martín, I. Zamora, F. J. Asensio, and O. Oñederra, "Analysis of the current electric battery models for electric vehicle simulation," *Energies*, vol. 12, no. 14, p. 2750, 2019.

[8] S. R. Jape and A. Thosar, "Comparison of electric motors for electric vehicle application," *international Journal of Research in Engineering and Technology*, vol. 6, no. 09, pp. 12–17, 2017.

[9] F. P. Beer, E. R. Johnston, J. T. DeWolf, and D. F. Mazurek, *Statics and mechanics of materials*. McGraw-Hill Education, 2021.

[10] R. Y. Garud and A. Pandey, "Structural analysis of automotive chassis, design modification and optimization," *Int. J. Appl. Eng. Res*, vol. 13, no. 11, pp. 9887–9892, 2018.

[11] A. Robinson and A. Livesey, *The repair of vehicle bodies*. Routledge, 2013.

[12] D. Prasetiyo *et al.*, "Strenght analysis chassis of um electric cars using finite element method," in *MATEC Web of Conferences*, vol. 204, p. 07017, EDP Sciences, 2018.

[13] M. S. bin Ab Razak, M. H. bin Hasim, and N. A. bin Ngatiman, "Design of electric vehicle racing car chassis using topology optimization method," in *MATEC Web of Conferences*, vol. 97, p. 01117, EDP Sciences, 2017.

[14] S. Nandhakumar, S. Seenivasan, A. M. Saalih, and M. Saifudheen, "Weight optimization and structural analysis of an electric bus chassis frame," *Materials Today: Proceedings*, vol. 37, pp. 1824–1827, 2021.

[15] H. Zhang, G. Huang, and D. Yu, "Numerical modeling for the frame structure of light van-type electric truck," *Science Progress*, vol. 103, no. 2, p. 0036850420927204, 2020.

[16] R. Rajappan and M. Vivekanandhan, "Static and modal analysis of chassis by using fea," *International Journal of Engineering and Science*, vol. 2, no. 2, pp. 63–73, 2013.

[17] T. Kristyadi, T. Shantika, L. Hartawan, *et al.*, "Stress analysis of a cross over electric car chassis," *IOSR Journal of Mechanical and Civil Engineering (IOSR-JMCE)*, vol. 14, no. 5, pp. 13–28, 2017.

[18] S. Durgam, V. M. Deshmukh, A. P. Jagtap, M. J. Sable, and N. M. Gawai, "Experimental and numerical studies on materials for electric vehicle chassis," in *IOP Conference Series: Materials Science and Engineering*, vol. 1126, p. 012073, IOP Publishing, 2021.

[19] A. H. Kishan and P. Kondalarao, "Transient structural analysis of electric bus chassis frame," in *IOP Conference Series: Materials Science and Engineering*, vol. 1185, p. 012038, IOP Publishing, 2021.

[20] S. Widyanto, O. Kurdi, G. Haryadi, I. Haryanto, and M. Rokhim, "Stress analysis of electric bus chassis using finite element method," in *Journal of Physics: Conference Series*, vol. 1321, p. 022014, IOP Publishing, 2019.

[21] R. Diary Ali, "Design and development of a chassis concept for an autonomous airport shuttle," 2020.

[22] W. B. Riley and A. R. George, "Design, analysis and testing of a formula sae car chassis," tech. rep., SAE Technical Paper, 2002.

[23] T. M. Corporation., “Overview: Profile: Company.”

[24] “Tmc hiace quality built for the world.”

[25] Z. Wang, T. W. Ching, S. Huang, H. Wang, and T. Xu, “Challenges faced by electric vehicle motors and their solutions,” *IEEE Access*, vol. 9, pp. 5228–5249, 2020.

[26] X. Hu, C. Zou, C. Zhang, and Y. Li, “Technological developments in batteries: a survey of principal roles, types, and management needs,” *IEEE Power and Energy Magazine*, vol. 15, no. 5, pp. 20–31, 2017.

[27] B. Coovert, *Research and Development of Electric Micro-Bus Vehicle Chassis*. PhD thesis, Purdue University Graduate School, 2023.

[28] M. F. Ashby and D. Cebon, “Materials selection in mechanical design,” *MRS Bull*, vol. 30, no. 12, p. 995, 2005.

[29] W. when how, “Chassis frame design (automobile).”

[30] L. e media, “Welcome to sajha yatayat: Public transportation in nepal.”

[31] Btiernay, “Grade guide: A36 steel,” Mar 2021.

[32] R. G. O. Nandan, S. Shashank, and D. Irwin, “A journal on “design and optimization of vehicle chassis for harsh road conditions”,” 2022.

[33] W. when how, “Chassis frame sections (automobile).”

[34] A. Sharma, P. Kumar, A. Jabbar, and M. M. Khan, “Structural analysis of a heavy vehicle chassis made of different alloys by different cross sections,” *International Journal of Engineering Research & Technology (IJERT)*, vol. 3, no. 6, pp. 1778–1785, 2014.

[35] P. Baral, R. Shrestha, R. N. Shrestha, D. Banstola, and R. Prajapati, “A study of height, weight and body mass index in nepalese,” *Journal of Gandaki Medical College-Nepal*, vol. 14, no. 2, pp. 88–92, 2021.

[36] L. A. Kareem, “Shear force bending moment.”

[37] “Tyre speed rating - tyre tips - finixx tyre,” Feb 2016.

[38] S. Bhavikatti, *Design of Steel Structures (By Limit State Method As Per Is: 800 2007)*. IK International Pvt Ltd, 2009.

[39] J. Zhang and W. Ran, "Lightweight optimization design of a light electric commercial vehicle frame," in *Journal of Physics: Conference Series*, vol. 1939, p. 012038, IOP Publishing, 2021.

APPENDIX A

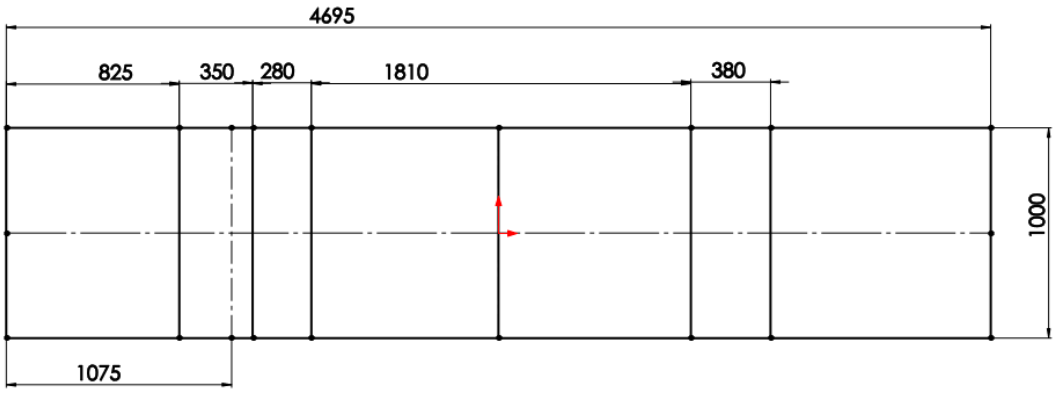

Figure 6.1: line sketch of chassis frame

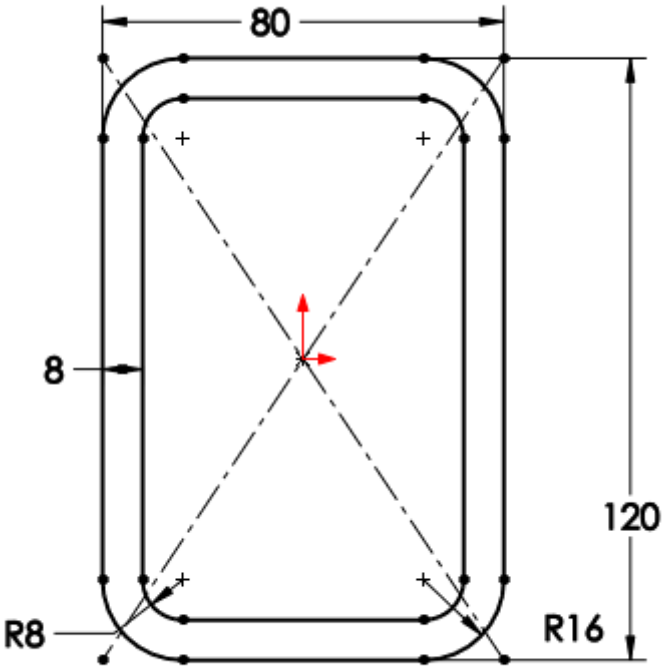

Figure 6.2: Weldment profile RHS 120*80*8 for two long side members

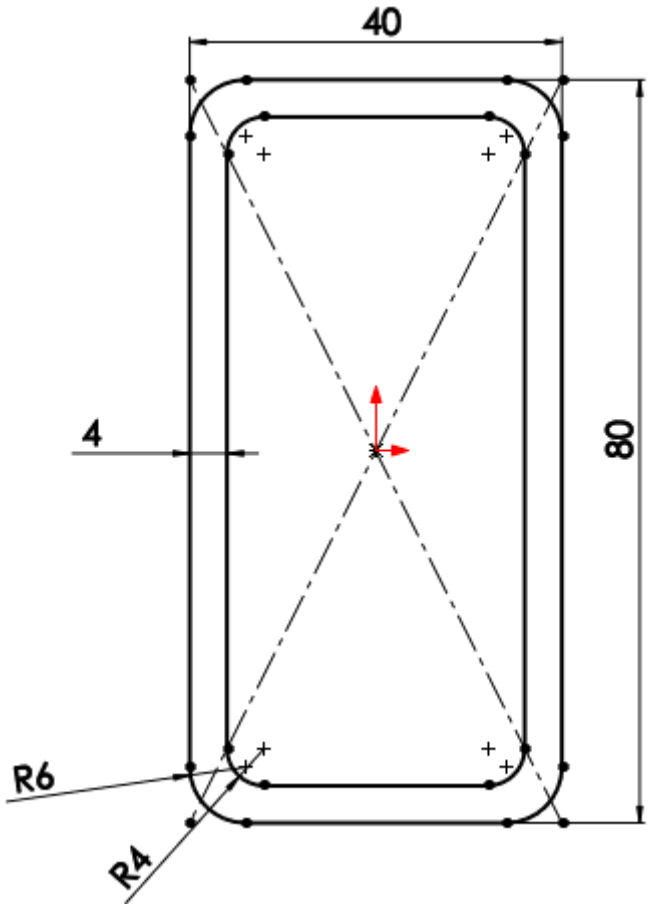

Figure 6.3: Weldment profile RHS 80*40 /4 for middle cross-members

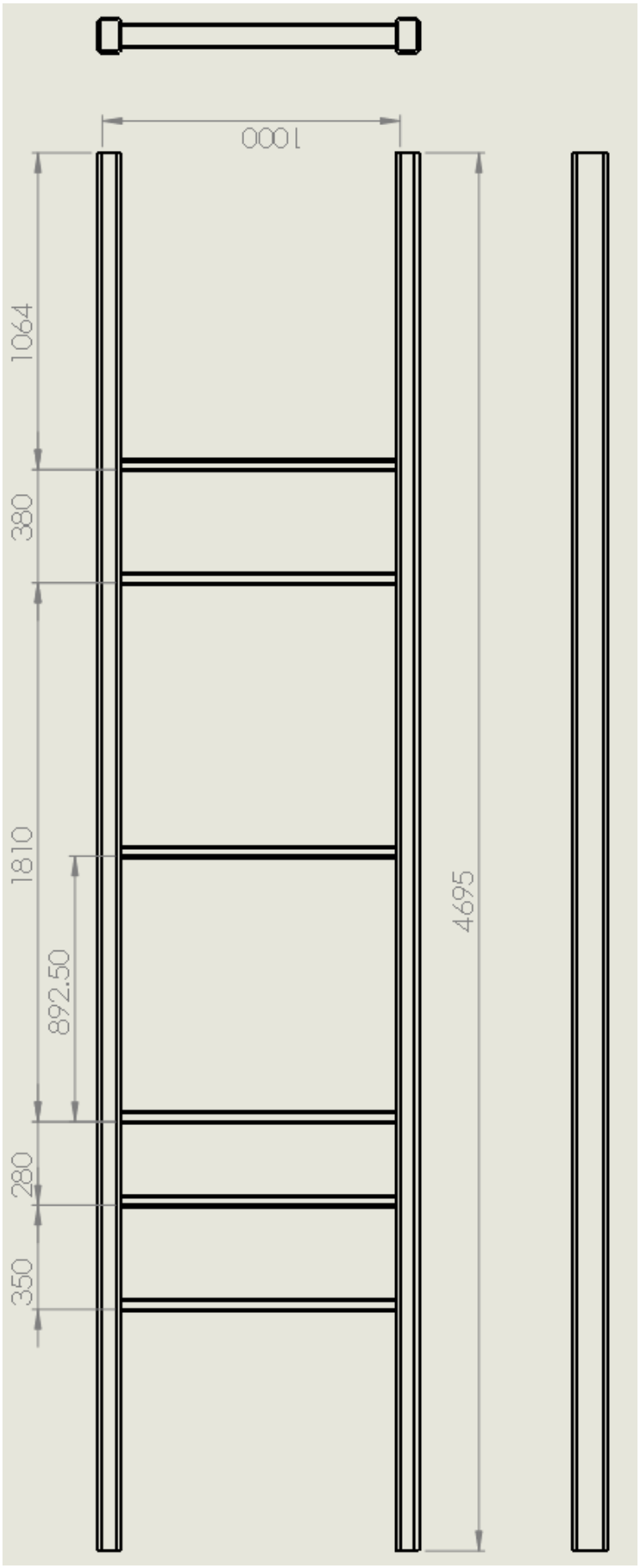

Figure 6.4: Three standard views of chassis frame

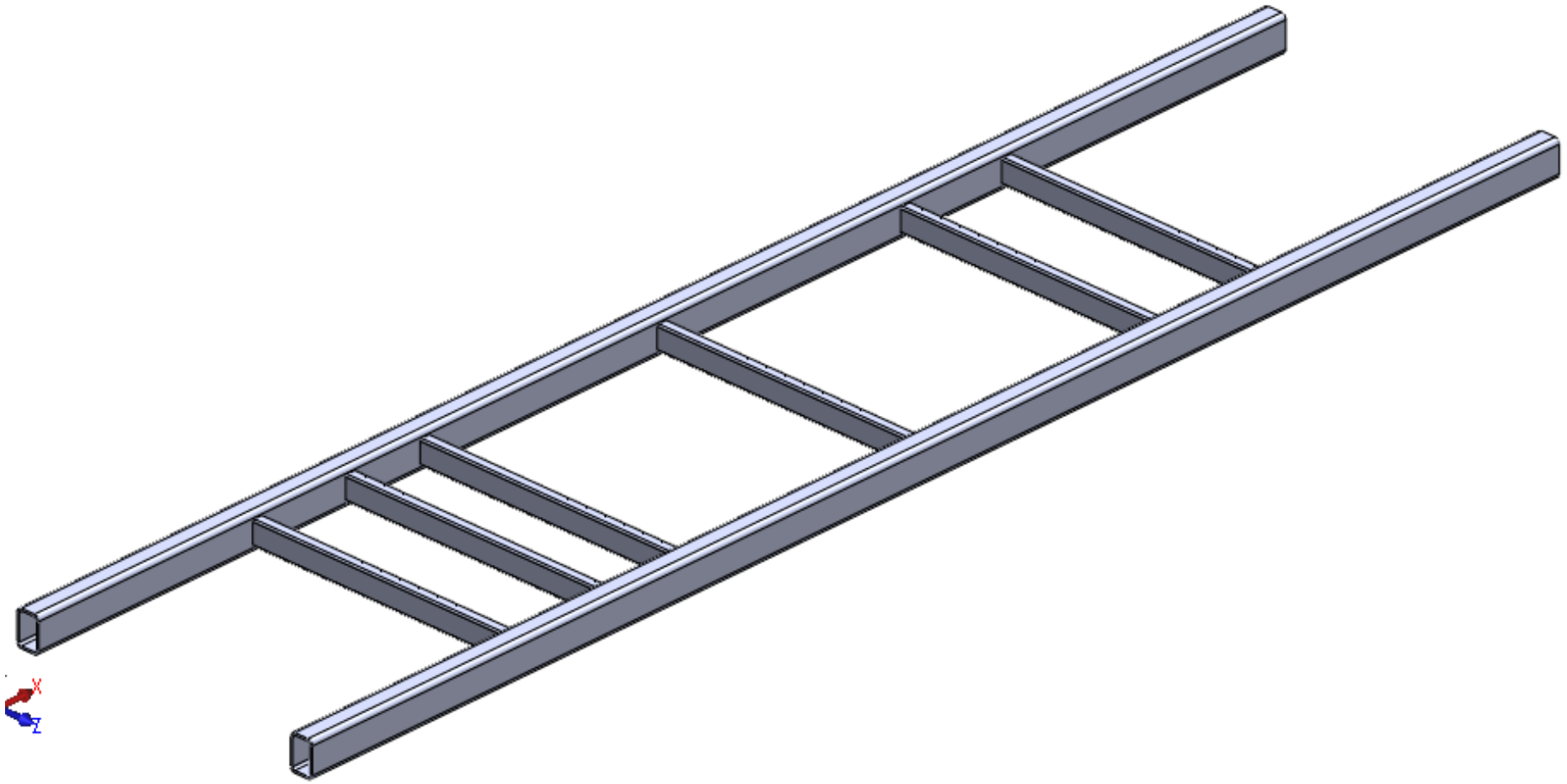

Figure 6.5: 3D view of the model

APPENDIX B

Table of design properties for rectangular steel profiles-Rectangular Hollow Sections

Profile	Depth	Width	Wall thick-ness	Outer round-ing ra-dius	Inner round-ing ra-dius	Second mo-ment of area	Radius of gy-ration	Elastic sec-tion mod-ulus	Plastic sec-tion mod-ulus
	h	b	t	ro	ri	Iy	iy	Wel,y	Wpl,y
	[mm]	[mm]	[mm]	[mm]	[mm]	[$\times 10^6$ mm^4]	[mm]	[$\times 10^3$ mm^3]	[$\times 10^3$ mm^3]
RHS 50x30 / 2.6	50	30	2.6	3.9	2.6	0.1218	17.9	4.873	6.118
RHS 50x30 / 3.2	50	30	3.2	4.8	3.2	0.1421	17.6	5.683	7.246
RHS 50x30 / 4	50	30	4	6	4	0.1649	17.2	6.596	8.593
RHS 50x30 / 5	50	30	5	7.5	5	0.1871	16.7	7.486	10.03
RHS 60x40 / 2.6	60	40	2.6	3.9	2.6	0.2358	22	7.862	9.649
RHS 60x40 / 3.2	60	40	3.2	4.8	3.2	0.2782	21.8	9.275	11.52
RHS 60x40 / 4	60	40	4	6	4	0.3283	21.4	10.94	13.83
RHS 60x40 / 5	60	40	5	7.5	5	0.3809	20.9	12.7	16.39
RHS 60x40 / 6.3	60	40	6.3	9.4	6.3	0.4339	20.2	14.46	19.23
RHS 80x40 / 3.2	80	40	3.2	4.8	3.2	0.5718	28.3	14.3	18.04
RHS 80x40 / 4	80	40	4	6	4	0.682	27.9	17.05	21.82
RHS 80x40 / 5	80	40	5	7.5	5	0.8028	27.4	20.07	26.13
RHS 80x40 / 6.3	80	40	6.3	9.4	6.3	0.9328	26.7	23.32	31.08
RHS 80x40 / 8	80	40	8	12	8	1.06	25.8	26.5	36.47
RHS 90x50 / 3.2	90	50	3.2	4.8	3.2	0.8913	32.5	19.81	24.56
RHS 90x50 / 4	90	50	4	6	4	1.071	32.1	23.8	29.85
RHS 90x50 / 5	90	50	5	7.5	5	1.273	31.6	28.28	35.99
RHS 90x50 / 6.3	90	50	6.3	9.4	6.3	1.499	31	33.3	43.22
RHS 90x50 / 8	90	50	8	12	8	1.736	30.1	38.57	51.41

RHS 100x50 / 3.2	100	50	3.2	4.8	3.2	1.159	35.7	23.17	28.94
RHS 100x50 / 4	100	50	4	6	4	1.396	35.3	27.92	35.24
RHS 100x50 / 5	100	50	5	7.5	5	1.665	34.8	33.3	42.61
RHS 100x50 / 6.3	100	50	6.3	9.4	6.3	1.971	34.2	39.42	51.35
RHS 100x50 / 8	100	50	8	12	8	2.299	33.3	45.98	61.38
RHS 100x60 / 3.2	100	60	3.2	4.8	3.2	1.309	36.7	26.17	32.04
RHS 100x60 / 4	100	60	4	6	4	1.58	36.3	31.61	39.08
RHS 100x60 / 5	100	60	5	7.5	5	1.891	35.8	37.82	47.36
RHS 100x60 / 6.3	100	60	6.3	9.4	6.3	2.248	35.2	44.96	57.25
RHS 100x60 / 8	100	60	8	12	8	2.638	34.4	52.77	68.74
RHS 120x60 / 4	120	60	4	6	4	2.487	42.8	41.46	51.87
RHS 120x60 / 5	120	60	5	7.5	5	2.992	42.3	49.87	63.09
RHS 120x60 / 6.3	120	60	6.3	9.4	6.3	3.583	41.6	59.71	76.66
RHS 120x60 / 8	120	60	8	12	8	4.247	40.8	70.79	92.7
RHS 120x60 / 10	120	60	10	15	10	4.881	39.7	81.36	109.2
RHS 120x80 / 4	120	80	4	6	4	3.026	44.6	50.43	61.15
RHS 120x80 / 5	120	80	5	7.5	5	3.654	44.2	60.9	74.59
RHS 120x80 / 6.3	120	80	6.3	9.4	6.3	4.398	43.6	73.3	90.98
RHS 120x80 / 8	120	80	8	12	8	5.253	42.7	87.54	110.6
RHS 120x80 / 10	120	80	10	15	10	6.095	41.8	101.6	131.2
RHS 140x80 / 4	140	80	4	6	4	4.406	51.2	62.94	77.14
RHS 140x80 / 5	140	80	5	7.5	5	5.34	50.8	76.28	94.32